

Journal of Geophysical Research: Space Physics

RESEARCH ARTICLE

10.1002/2016JA023381

Key Points:

- Eastward and westward QTDWs in all meteorological fields have been studied in hourly NOGAPS-ALPHA reanalysis data
- At middle-/high-latitude E2 and E3 waves are observed in winter hemisphere, while W2, W3, and W4 waves are observed in summer hemisphere
- At low latitudes E2 wave (not in meridional wind) is ultrafast Kelvin waves, while W1, W2, and W3 in meridional wind are Rossby-gravity modes

Correspondence to:

D. Pancheva,
dpancheva@geophys.bas.bg

Citation:

Pancheva, D., P. Mukhtarov, D. E. Siskind, and A. K. Smith (2016), Global distribution and variability of quasi 2 day waves based on the NOGAPS-ALPHA reanalysis model, *J. Geophys. Res. Space Physics*, 121, 11,422–11,449, doi:10.1002/2016JA023381.

Received 22 AUG 2016

Accepted 29 OCT 2016

Accepted article online 2 NOV 2016

Published online 16 NOV 2016

Global distribution and variability of quasi 2 day waves based on the NOGAPS-ALPHA reanalysis model

Dora Pancheva¹, Plamen Mukhtarov¹, David E. Siskind², and Anne K. Smith³

¹National Institute of Geophysics, Geodesy and Geography, BAS, Sofia, Bulgaria, ²Space Science Division, Naval Research Laboratory, Washington, District of Columbia, USA, ³Atmospheric Chemistry Observations and Modeling, National Center for Atmospheric Research, Boulder, Colorado, USA

Abstract This study presents the analysis of 14 months (January 2009 to February 2010) of continuous hourly Navy Operational Global Atmospheric Prediction System-Advanced Level Physics High Altitude reanalysis data used for examining the quasi 2 day wave (QTDW). The global structure and seasonal variability of the eastward and westward traveling QTDWs in all meteorological fields (geopotential height, zonal and meridional wind, and temperature) have been studied. The use of hourly reanalysis data allows a comprehensive understanding of the global spatial-temporal QTDW distribution by simultaneous separations of all tides and planetary waves. The wave characteristics (amplitudes and phases) are presented in latitude range $\pm 80^\circ$ and altitudes from 15 to 95 km. Two different types of eastward traveling waves are identified: (i) waves at middle and high latitudes with zonal wave numbers 2 and 3, which are observed in the local winters, and (ii) waves observed predominantly over the equator with zonal wave number 2, which do not have a well-defined seasonal variability but show some enhancement between June and August. While the first type waves are seen in all meteorological fields, the second ones are not seen in the meridional wind and belong to the ultrafast Kelvin waves. Two different types of westward traveling waves have been identified as well: (i) waves at middle and high latitudes with zonal wave numbers 2, 3, and 4, which are observed mainly in summer hemisphere, and (ii) waves observed predominantly over the equator with zonal wave numbers 1, 2, and 3, enhanced predominantly at both solstices but are seen in other seasons as well. While the first type waves are seen in all meteorological fields, the second ones are observed in the meridional wind and are Rossby-gravity normal modes.

1. Introduction

The quasi 2 day wave (QTDW) is one of the most prominent planetary wave phenomena in the middle atmosphere with a quite long history of exploration. The wave observations have been extensively reported by ground-based radars [Muller, 1972; Craig et al., 1980; Raghava Reddi et al., 1988; Harris and Vincent, 1993; Palo and Avery, 1995; Thayaparan et al., 1997; Gurubaran et al., 2001a; Lima et al., 2004; Pancheva, 2006], rocketsondes in the upper stratosphere [Coy, 1979] satellite observations [Rodgers and Prata, 1981; Burks and Leovy, 1986; Wu et al., 1993; Ward et al., 1996; Lieberman, 1999; Garcia et al., 2005; Limpasuvan et al., 2005; Tunbridge et al., 2011; Gu et al., 2013], and in a number of multi-instrument observational campaigns as well [e.g., see Pancheva et al., 2004a, and references therein].

The classical picture of the QTDW is that it is a summertime phenomenon at middle latitudes, typically maximizing in the month after solstice. In the Northern Hemisphere (NH), the largest wave amplitudes are observed near the mesopause in July–August, and there is a corresponding Southern Hemisphere (SH) maximum in January–February. The observed QTDWs are mainly westward propagating with zonal wave number 3 (W3) or 4 (W4), and the W3 is generally much stronger (nearly twice) than W4 in the SH, while in the NH the W4 wave, according to Tunbridge et al. [2011], is usually stronger than W3. A small-amplitude westward traveling zonal wave number 2 (W2) wave has also been reported [Meek et al., 1996; Norton and Thuburn, 1996].

In addition to the summertime QTDW, and of particular interest for the present paper, are middle atmospheric waves with a period near 2 days but observed in winter middle to high latitudes. These have been seen in radar neutral wind data covering the mesosphere and lower thermosphere (MLT) region [Nozawa et al., 2003; Manson et al., 2004]. However, due to the localized nature of the measurements, these studies

were unable to determine the zonal wave structure of this wave. Also uncertain is the direction of propagation. Simultaneous wind measurements made by *Merzlyakov et al.* [2005] at two Arctic locations however gave evidence for a strong eastward traveling QTDW in the winters of 1999/2000 and 2000/2001 with zonal wave number 2. To more definitively remove any ambiguity associated with ground based measurements, *Merzlyakova and Pancheva* [2007] combined the Esrange (21°E, 68°N) meteor wind data with temperature measurements from the Sounding of the Atmosphere using Broadband Emission Radiometry (SABER) instrument on board the thermosphere-ionosphere-mesosphere energetics and dynamics (TIMED) spacecraft. They found significant pressure, temperature, and wind oscillations with period of ~2 days propagating eastward with zonal wave number 2 during February 2004. Later, *Sandford et al.* [2008] by using geopotential height data from the Microwave Limb Sounder (MLS) instrument on board the NASA Aura satellite for the interval August 2004 to November 2007 supported *Merzlyakova and Pancheva* [2007] finding for the QTDW, i.e., that the winter polar mesosphere is dominated by an eastward traveling 2 day E2 wave. It is worth noting however that satellite studies of planetary waves can be complicated by aliasing because the longitude and local time of observations are not independent [*Wu et al.*, 1995].

It is known that the QTDW can attain large amplitudes particularly in the meridional wind component in the equatorial MLT region. The ground-based observations in the equatorial and low latitudes [*Kal'chenko and Bulgakov*, 1973; *Harris and Vincent*, 1993; *Palo and Avery*, 1995; *Gurubaran et al.*, 2001a; *Lima et al.*, 2004; *Pancheva et al.*, 2004b] indicated that the activity is stronger in both summer and winter in the meridional component and was found to be much stronger in January–February than in June–July with maximum around 90–95 km. Using the High Resolution Doppler Imager, *Wu et al.* [1993] found a strong QTDW W3 peak of ~60 m/s in the meridional component around 100 km near the equator in January. Later, *Ward et al.* [1996] and *Niciejewski et al.* [2011] using different satellite meridional wind measurements confirmed the existence of such a QTDW W3 peak in meridional wind near the equator in the lower thermosphere.

Our current understanding of the QTDW describes the wave as a combination of a resonant mode [*Salby*, 1981a, 1981b] that is amplified by instabilities in the summertime mesospheric easterly jet [*Plumb*, 1983]. The relative invariance of the observed period and overall spatial structure are therefore tied to the existence of the gravest Rossby-gravity (3, 0) normal mode for the west traveling zonal wave number 3 wave. The summertime enhancement results from barotropic/baroclinic instability on the poleward edge of the jet around 50–60°N [*Pfister*, 1985]. This dual nature particularly valid for W3 mode has been borne out by more recent work [*Salby and Callaghan*, 2001; *Palo et al.*, 2007; *Yue et al.*, 2012; *Gu et al.*, 2015].

As noted above, in addition to the dominant W3 mode, other westward traveling wave modes are present. The summertime W4 mode, first reported by *Rodgers and Prata* [1981], also seems linked to the unstable region of the summer easterly jet [*Plumb*, 1983]. Analyses of satellite data have documented the relatively interannual variability of the W3 and W4 components [*Tunbridge et al.*, 2011; *Gu et al.*, 2013]. They tend to show that the W4 reaches the largest amplitude when the W3 mode is weak; this may explain why it tends to be stronger in the NH, whereas the W3 mode is generally stronger in the SH. *Gu et al.* [2013] suggested that W4 mode is likely related to the occurrence of a relatively weaker summer easterly jet that is not able to provide sufficiently strong barotropic/baroclinic instability to amplify W3 but is favorable for the amplification of W4. As with the W3, the above mentioned observations of the W4 showed good agreement with a Rossby-gravity (4, 0) mode. Finally, there is a 2 day W2 mode that is much weaker than both W3 and W4 modes. This was associated by *Rojas and Norton* [2007] with a wave signal with wave number 2 and period of 49 h found in a linear 2-D instability model indicating that the W2 could be an unstable wave. *Riggin et al.* [2004] investigated particularly the meridional wind component of W2 in the boreal summer and reported that it is more symmetric with respect to the equator than W3, that the W2 mode propagates equatorially from high latitudes and it could be excited in situ at high latitudes. *Gu et al.* [2015] found that the W2 could also be forced by the nonlinear interaction between the W3 and the stationary planetary wave 1 (SPW1).

Finally, *Ito et al.* [1986] first theoretically suggested that a large-amplitude global-scale QTDW can induce an electric current system in the ionosphere through a dynamo mechanism. *Pancheva and Lysenko* [1988] first identified the signatures of the quasi 2 day variability in the maximum electron density of the ionospheric F region and showed a high correlation with the 2 day wave measured by the meteor radar situated close to the ionosonde station. This result has been supported later by many observations reporting quasi 2 day signatures in the ionosphere [*Chen*, 1992; *Pancheva et al.*, 1994; *Apostolov et al.*, 1995; *Forbes et al.*, 1997;

Altadill and Apostolov, 1998; Gurubaran et al., 2001b; Pancheva et al., 2006]. This indicates the important role of the QTDW event not only for the dynamics of the middle atmosphere but also for the coupling process in the atmosphere-ionosphere system. Cautions however must be taken when comparing QTDWs in the mesosphere and ionosphere in terms of wave number. Yue et al. [2013] shows that during the mapping process from geographic ordinates into geomagnetic field, additional wave numbers can be introduced.

Both of the historical approaches to studying the QTDW have inherent limitations. The ground-based methods can provide a detailed temporal variability of the QTDW however cannot provide insight into its global distribution. Satellite measurements can do this; however, they suffer from aliasing and poor temporal resolution problems. Most recently, meteorological analyses have been used to study the QTDW [McCormack et al., 2009]. A synoptic analysis can overcome the limitations of both ground-based and satellite observations. Here we employ a version of the Navy Operational Global Atmospheric Prediction System-Advanced Level Physics High Altitude (NOGAPS-ALPHA) reanalysis model that has been configured to supply output on an hourly basis. It allows for short-term, observationally based, estimates of tides, and planetary waves to be performed. This can be particularly valuable in light of suggestions by *Walterscheid and Vincent [1996]* and, later, *McCormack et al. [2010]* that the QTDW can be nonlinearly resonant with thermal tides. We analyze 14 months (January 2009 to February 2010) continuous hourly measurements of all meteorological fields (neutral winds, temperature, and geopotential height) for altitudes between ~15 and ~95 km and latitudes between $\pm 80^\circ$. The basic aim of the present paper is to examine in detail the global structure and seasonal variability of the eastward and westward traveling QTDWs observed in all NOGAPS-ALPHA reanalysis fields during the considered time interval.

2. NOGAPS-ALPHA Reanalysis Fields and Data Analysis

2.1. Data

All QTDW results obtained from the satellite measurements, so far, have been obtained by separation from the data of only QTDWs. If, however, the forcing [*Walterscheid and Vincent, 1996*] or enhancement [*McCormack et al., 2010; Yue et al., 2012*] of the QTDW could be related to the atmospheric tides, and keeping in mind that the QTDWs are varying in time, then a correct way for examining the QTDWs is for these waves and atmospheric tides to be extracted from the data concurrently. To facilitate the simultaneous analysis of planetary waves and tides, we utilize the Advanced Level Physics High Altitude version of the Navy Operational Global Atmospheric Prediction System (NOGAPS-ALPHA) reanalysis model.

NOGAPS-ALPHA was developed as a prototype vertical extension of the U.S. Navy's operational-forecast model. *Eckermann et al. [2009]* discuss the additional physical parameterizations added to extend the forecast model up to approximately 90 km. The data assimilation component of NOGAPS-ALPHA is the Naval Research Laboratory Atmospheric Variational Data Assimilation System (NAVDAS). NAVDAS is a 3D-variational system with a 6-hourly update cycle that assimilates both conventional meteorological data as well as data from the Aura Microwave Limb Sounder (MLS) and SABER. These analysis have been used successfully to describe the large-scale circulation of the mesosphere with period greater than 12 h [*Coy et al., 1980; Siskind et al., 2011; McCormack et al., 2009, 2010; Nielsen et al., 2010; Stevens et al., 2010*]. One limitation of NAVDAS is that the 6-hourly update cycle may alias semidiurnal and higher-order tidal modes. To circumvent this, a version of the NOGAPS ALPHA forecast model was configured to be initialized every 6 h from the analysis but provide output on an hourly cadence [*Siskind et al., 2012*]. *Lieberman et al. [2015]* have used this version of NOGAPS-ALPHA to study nonmigrating tides.

2.2. The 2-D Wavelet Analysis

Usually, planetary waves are transient phenomena, i.e., the data contain nonstationary power at many different frequencies. This is particularly valid for the QTDWs which are burst-like events. Thus, time-frequency analyses, as, e.g., the wavelet transform, have to be applied. The 2-D wavelet transform enables the determination of both which modes of variability are dominant and how these modes vary in time and space. Details about the 2-D wavelet transform used in this work can be found in *Mukhtarov et al. [2010]*. Our preliminary analysis reveals that both westward and eastward traveling QTDWs are seen in the meteorological fields. At middle and high latitudes the westward traveling waves are present in the local summer, while the eastward traveling ones are observed in the local winter. Figure 1a shows the wavelet spectra of the W2 (upper row), W3 (middle row), and W4 (bottom row) 2 day waves observed in the geopotential height

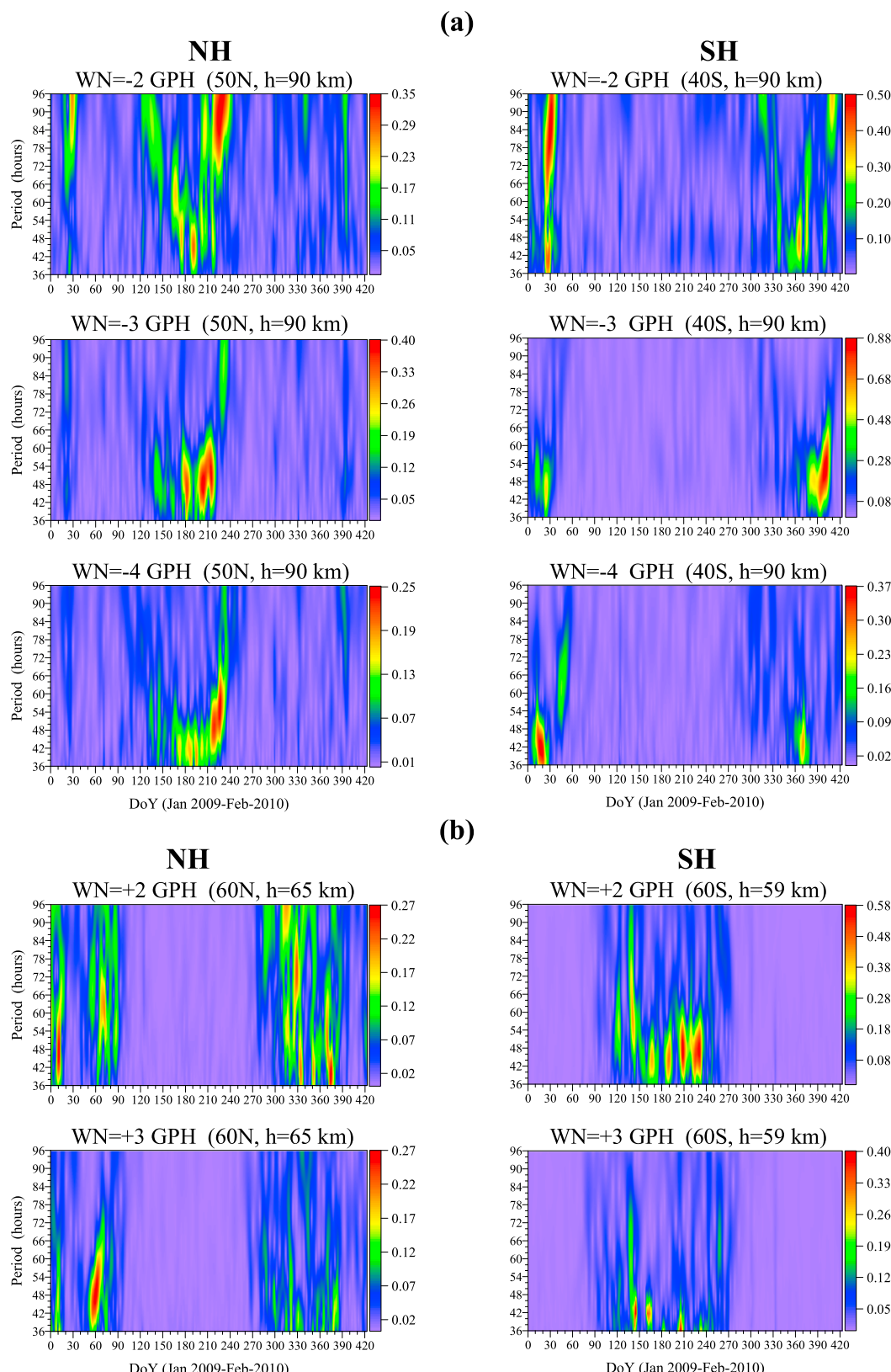


Figure 1. (a) Two-dimensional wavelet spectra of the W2 (top row), W3 (middle row), and W4 (bottom row) 2 day waves observed in the GPH data for latitude of 50°N and altitude of 90 km (left column) and latitude of 40°S and altitude of 90 km (right column); (b) the same as Figure 1a but for the E2 (top row) and E3 (bottom row) 2 day waves for latitude of 60°N and altitude of 65 km (left column) and latitude of 60°S and altitude of 59 km (right column).

(GPH) data. The NH wavelet spectra are shown for latitude of 50°N and altitude of 90 km (left column), while those of the SH are for latitude of 40°S and altitude of 90 km (right column). The spectra are presented for periods between 36 and 96 h (1.5–4 days) and are calculated for the entire interval of 14 months. The NH spectral peaks for these zonal numbers display a regular variability from larger periods in April to shortest periods in July and then again the period increases to early September. Focusing just on the June–August period, we see that the average periods for the different zonal wave numbers are slightly different: ~50 h for W2, close to 48 h for W3 and ~44 h for W4 wave. The westward traveling waves in the SH are observed predominantly in January–February 2009 and 2010. In this case the tendency for decreasing period with increasing wave number is not well visible; the mean periods for W2 and W3 waves are ~45 h in January 2009 and ~50 h for January–February 2010, while for the W4 wave it is ~45–46 h.

Figure 1b presents the wavelet spectra of the eastward traveling QTDWs in the GPH data for both hemispheres. The spectra for the E2 wave are shown in Figure 1b (top row), while those for the E3 wave are in Figure 1b (bottom row). The NH wavelet spectra are shown for latitude of 60°N and altitude of 65 km (left column), while those of the SH are for latitude of 60°S and altitude of 59 km (right column). The E2 and E3 waves in the NH are observed in the first half of January and at the end of February/March 2009 and during the next winter from the end of November to around 20 January 2009/2010. The mean periods for the E2 and E3 waves vary between the two winters: while they are ~48–50 h in the first winter in second one they decrease to ~45 h. The absence of the 2 day wave peaks during ~20 January to ~20 February 2009 and from the end of January to the end of February 2010 coincides with the occurrence of the major sudden stratospheric warming (SSW) events in both winters. During SSW the zonal mean flow in the stratosphere changes its direction from eastward to westward, affecting instability and propagations conditions [Sandford *et al.*, 2008]. The E2 and E3 waves in the SH are seen in the local winter between the end of May to August. While the mean period of the E2 wave is ~48 h that of the E3, one is ~42–44 h.

We particularly note that the wave periods and intermittent behavior found in the wavelet results in the GPH data are valid also for all fields considered in this study, i.e., for zonal and meridional winds and temperature. In sections 3 and 4, where these QTDWs will be investigated in detail, their global distribution and temporal variability will be shown for all four variables. It is worth noting that the presence of the eastward traveling E3 wave has not been reported previously either in observations or in modeling studies.

Figure 2a displays the 2-D wavelet spectra of the W1 (top left), W2 (top right), and W3 (bottom) 2 day waves observed in the meridional wind over the equator (actually at latitude of 01°N) and altitude of 90 km. We note that the westward traveling QTDW over the equator is seen in the meridional but not zonal wind. The peaks of the W3 wave are strongest; they are enhanced in both solstices. For this period the strongest W3 wave is observed at the end of January/February 2010. The mean period is ~50–52 h. Later, it will be shown that the enhancements of the tropical W3 wave are related to the amplifications of the same W3 wave observed in midlatitudes; the January–February enhancement is related to the W3 wave in the SH summer while the June–July one to the W3 wave in the NH summer. The W1 and W2 spectra show some amplification in the solstices also when their amplitudes are larger, but it seems that these waves are more burst like than the W3 one. While the period of the W2 wave changes between ~48 and ~52 h, that of the W1 wave is shorter, on the average ~45 h. Later, it will be shown that the tropical W2 wave in the meridional wind can amplify during solstices, together with that in the summertime middle latitudes, but it exists during other periods as well. It is worth noting that the presence of the tropical westward traveling W1 and W2 waves has not been reported previously either in observations or in modeling studies. However, Pancheva *et al.* [2006] analyzed perturbations in the geomagnetic field measured in 23 stations situated at low latitudes and found 2 day variations in the ionospheric electric currents identified as westward propagating global 2 day waves with zonal wave numbers 1 and 2.

The preliminary investigations indicated that there is also an eastward traveling E2 wave over the equator seen in all meteorological fields except meridional wind. Figure 2b shows the 2-D wavelet spectra for the 2 day E2 wave observed in the GPH (top left), zonal wind (top right), and temperature (bottom plot). These spectra do not demonstrate clear seasonal behavior; however, all of them reveal enhanced peaks during June–August with periods of ~48 h for the temperature, ~48–52 h for the zonal wind, and ~45–48 h for the GPH data. Enhanced peaks are seen also in March–April with shorter period, ~40–42 h, and in November with

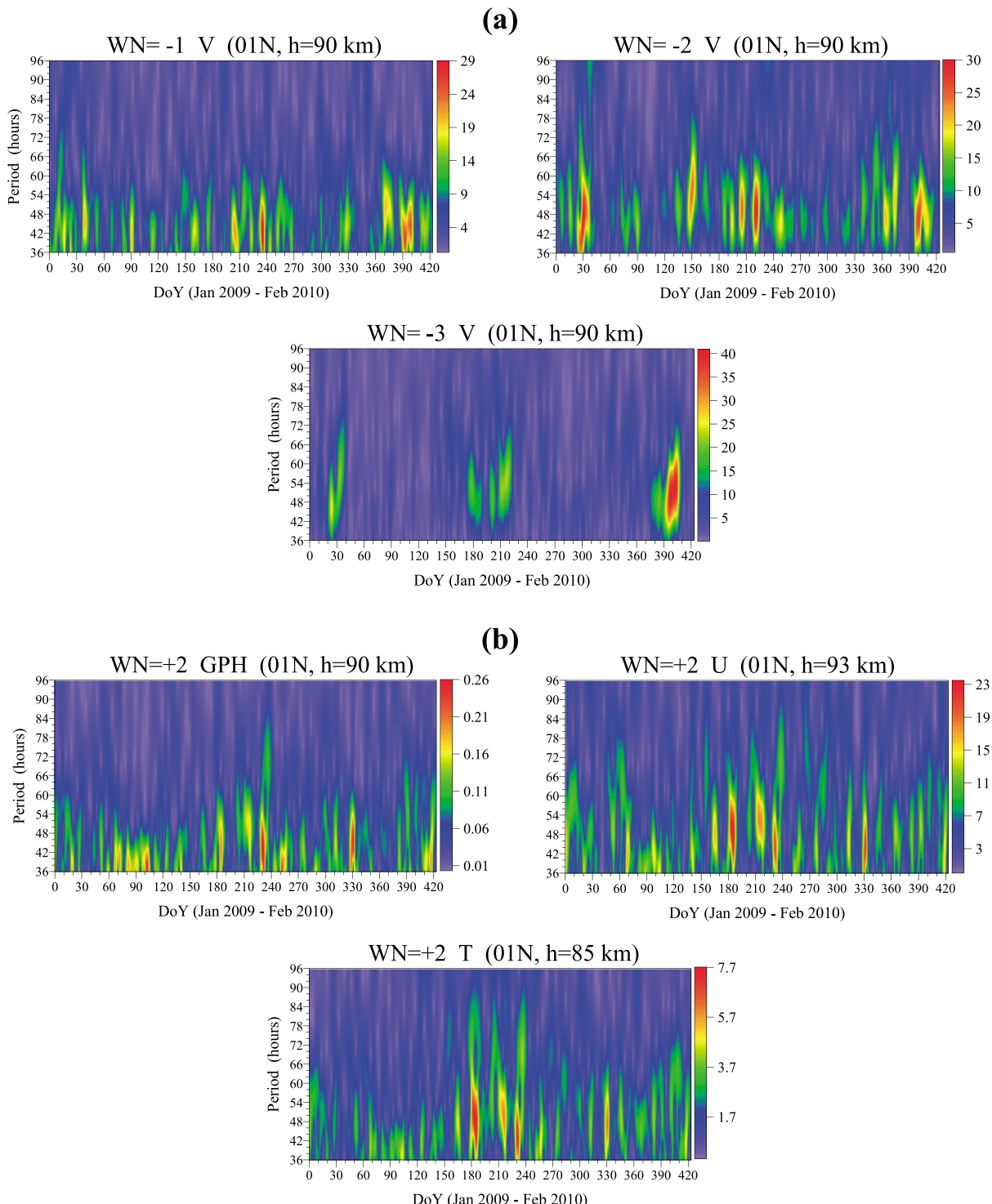


Figure 2. (a) Two-dimensional wavelet spectra of the W1 (top row, left), W2 (top row, right) and W3 (bottom) 2 day waves observed in the meridional wind for latitude of 01°N and altitude of 90 km; (b) the same as Figure 2a but for 2 day E2 wave observed in the GPH (top row, left), zonal wind (top row, right), and temperature (bottom).

a period of ~46–48 h. The eastward traveling E2 wave over the equator has not been previously reported. We note that there is a weak E3 wave over the equator, but it is at least 2.5–3 times weaker than the E2 wave and will not be examined in this study. The wavelet analysis indicated the presence of the E1 wave over the equator as well, but its mean period is ~3–3.5 days and will not be considered either.

The wavelet analysis revealed the existence of not only the already known summertime westward traveling W2, W3, and W4 waves but also the wintertime eastward traveling E2 and E3 QTDWs in the middle and high latitudes. For equatorial latitudes it demonstrated for the first time the presence of westward traveling W1 and W2 waves in the meridional wind and of eastward traveling E2 wave in the zonal wind, temperature, and GPH. It has been already mentioned that there are only a few references where the eastward traveling E2 wave particularly in the MLT region is studied. Besides *Merzlyakova and Pancheva [2007]* and *Sandford et al. [2008]*, the analysis by *Palo et al. [2007]* using SABER/TIMED temperature measurements reported an E2 wave in the midlatitude, summer SH MLT region occurring simultaneously with a W3 wave. The authors attributed the E2 wave to a nonlinear coupling between the W3 QTDW and the migrating diurnal tide. Later, *Moudden and Forbes [2014]*, also using SABER/TIMED data, examined the behavior of the E2 wave in relation to the W3 one and the generation of the secondary waves due to nonlinear interaction between W3, E2, and migrating diurnal and semidiurnal tides. However, as *Moudden and Forbes [2014]* pointed out, aliasing dominates uncertainties for all these waves. The W3 and E2 alias into each other at about 30% level near 40° latitude; the level of aliasing becomes less severe as one moves equatorward and more severe moving poleward. Nonetheless, on the basis of the differing vertical structure and interannual variability between the W3 and E2 waves, *Moudden and Forbes [2014]* concluded that the E2 wave was “real,” i.e., not the result of aliasing due to sampling. In our case here, the NOGAPS-ALPHA reanalysis data suffer the less from aliasing; hence, all 2 day wave peaks identified from the wavelet analysis correspond to real QTDWs, thus confirming *Moudden and Forbes [2014]* conclusion.

2.3. Separation of the QTDWs From the NOGAPS-ALPHA Data Sets

The wavelet analyses showed the presence of eastward and westward traveling QTDWs with different zonal structure and different periods mainly in the range between ~44 and ~56–58 h. The main purpose of this study is to examine the spatiotemporal distribution of all these waves existing in all meteorological fields: GPH, temperature, and horizontal winds. We need to perform spectral analysis using a fixed period in order to look at the global and vertical structure of the QTDW components. We choose a fixed period of 48 h for identifying the QTDWs in the data. Keep in mind that if a given QTDW has period different from 48 h, its amplitude will be slightly underestimated. In order to extract the QTDWs from the data, i.e., to determine their amplitudes and phases at a given latitude and altitude, we perform a linear two-dimensional (time-longitude) least squares fitting using a 6 day window that moves through the time series with steps of 1 day. In this way the daily characteristics of the waves are obtained. Besides the zonal mean (which is actually zonal and time mean in the frame of a window) the following waves are included in the fitting procedure: (i) all of the main tides with periods of 24, 12, and 8 h; (ii) 48 h waves; (iii) 6 day waves; and (iv) SPWs. For all waves we include zonal wave numbers up to 4. In order to remove some patchy structures with small amplitudes that may not be related to the QTDW event, an additional smoothing of the daily characteristics is done using a 15 day sliding time segment. The smoothing suppresses the wave amplitudes but gives a clearer view of the overall QTDW picture. The characteristics of the eastward traveling QTDWs are examined in section 3, while those of the westward traveling ones in section 4. It is worth noting that for studying all the above mentioned waves included in the decomposition procedure, we work in UT, i.e., UT and longitude are independent.

3. Eastward Traveling QTDWs

The 2-D wavelet analysis in Figure 1 revealed that the eastward traveling QTDWs in the middle and high latitudes are observed during the local winters. Propagation of planetary scale waves is dependent on the background zonal wind, in accordance with the Charney-Drazin criterion. Wintertime winds, especially in the NH, undergo frequent and rapid changes. The strongest of these are SSW events, during which middle atmosphere zonal winds in the middle and high latitudes of the NH reverse direction and resemble summer winds. Such changes of the zonal wind direction will affect the QTDWs.

3.1. Latitude Structure of the E2 and E3 Waves Observed in the Middle and High Latitudes

Figure 3 presents latitude-time cross sections of the 2 day E2 wave amplitudes in the GPH (first panel), meridional wind (second panel), zonal wind (third panel), and temperature (fourth panel) for the period of 01 January 2009 to 28 February 2010. The latitude structures of the E2 wave in the different fields are not necessarily displayed at altitudes where the E2 wave has the largest amplitude due to the following: (i) the E2 wave in all meteorological fields of the SH is significantly stronger than the respective wave in the NH and (ii) the

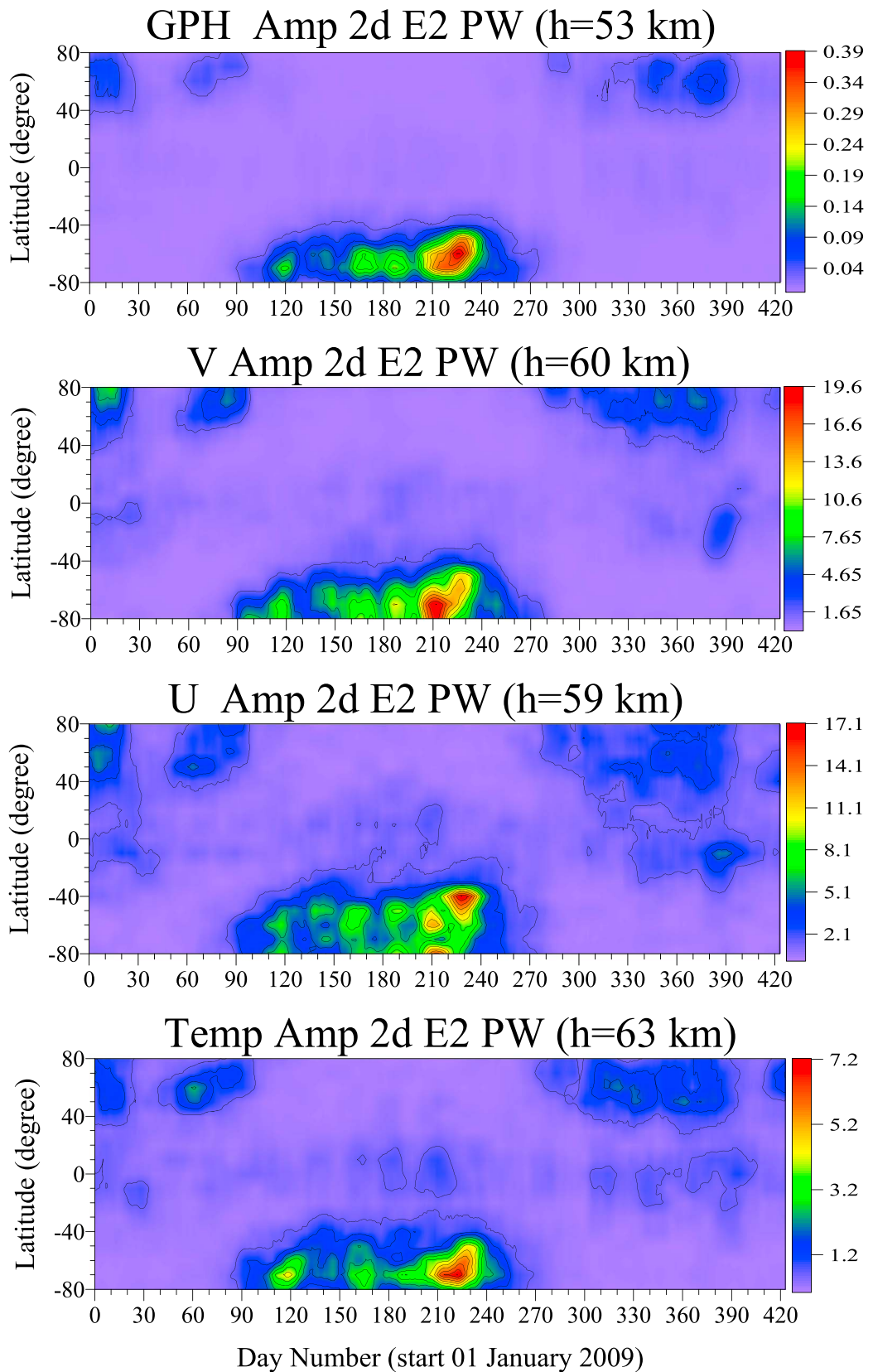


Figure 3. Latitude-time cross sections of the 2 day E2 wave amplitudes observed in the GPH (in km, first panel), meridional wind (in m/s, second panel), zonal wind (in m/s, third panel), and temperature (in K, fourth panel).

height where the E2 wave has the largest amplitude in all fields of the NH is situated higher than the respective one in the SH. Figure 3 displays the latitude structures at intermediate heights where the 2 day E2 wave are approximately well seen in both hemispheres. The first important feature of the E2 wave is that its temporal variability is very similar in all fields. Several synchronous bursts between days 110 and 240 are well seen in the SH, while in the NH similar bursts occur, but the presence of this wave is also interrupted by the two major SSW events occurred in 24 January 2009 and 26 January 2010. The mean zonal flow at level of 10 hPa was reversed for almost a month during the two major SSW events. The impact of the SSW on the 2 day E2 wave was reported first by *Sandford et al.* [2008], who analyzed MLS/Aura geopotential height measurements; the authors noticed that the wave is either not present or has small amplitudes. A careful inspection of all plots shows that the E2 wave amplifies at different latitudes, and this is particularly well seen in the SH; while the E2 wave in GPH and temperature has the largest amplitudes near $\sim 60\text{--}70^\circ\text{S}$, that in the meridional wind is largest around $\sim 70\text{--}80^\circ\text{S}$. The E2 wave in the zonal wind shows a double-peak latitudinal structure as the peaks are located at $\sim 40\text{--}50^\circ\text{S}$ and near 80°S . It is worth clarifying that the zonal wind double-peak structure is related to the single one in the GPH field because the zonal wind is proportional to the latitudinal gradient of the GPH (approximate geostrophic balance). Thus, the latitude of the each E2 wave peak in the GPH field (first panel) coincides approximately with the latitude of the minimum between the respective double-peak structure in the zonal wind (third panel).

Figure 4 displays the same as Figure 3 but for the 2 day E3 wave amplitudes. In this case the E3 wave in the NH is significantly stronger, particularly the peak at the end of February/March 2009, than that in the SH. Hence, its latitude structures at all meteorological fields are shown also at heights where they are approximately well seen in both hemispheres. Similarly to the E2 wave, here also the E3 temporal variability is very similar in all fields. The amplification of the E3 wave however is observed at similar latitudes, $\sim \pm 50^\circ$ for all meteorological fields except in the zonal wind. The presence of a double-peak latitude structure of the zonal wind E3 wave is particularly well seen in the NH; the E3 wave peaks are situated at $\sim \pm 40^\circ$ and $\sim \pm 60^\circ$. The impact of the two major SSW events on the presence of the 2 day E3 wave is also well seen; the wave disappears when the winter circulation in high latitudes is replaced by circulation that resembles a summer one.

3.2. Altitude Structure of the E2 and E3 Waves Observed in the Middle and High Latitudes

Figure 5 shows the altitude-time cross sections of the 2 day E2 wave amplitudes observed in the GPH (first row), meridional wind (second row), zonal wind (third row), and temperature (fourth row) for the latitudes of the NH (left column) and SH (right column) which are marked at the upper side of each plot. The altitude structures in the different meteorological fields are displayed at latitudes where the E2 wave has the largest amplitude. It has been already mentioned that the E2 wave is significantly stronger (more than a factor of 2) in the SH in all meteorological fields. Due to this, its altitude structure is very well outlined, i.e., the height where the wave has the largest amplitude is well evident in all fields. The 2 day E2 wave event in the SH (right column) consists of several peaks; the last one, seen between days 210 and 240 (August 2009), is the strongest. Its largest amplitude in the considered fields is 0.38 km in the GPH, 20 m/s in the meridional wind, 16.2 m/s in the zonal wind, and 7.1 K in the temperature. While the E2 maximum in the GPH is situated at altitude of ~ 52 km those in the meridional and zonal winds are at ~ 57 km and ~ 60 km, respectively. The E2 wave in the temperature shows a double-peak altitude structure, and the maxima are at altitudes of ~ 45 and ~ 60 km. We note that the relationship between the double-peak structure in the temperature and the single one in the amplitude of the GPH E2 wave is based on the hydrostatic equation, $T = (H/R)\Phi_z$, where R is the gas constant of dry air, H is the atmospheric scale height, and subscript z indicates vertical derivative, which is now well known and described by *Sassi et al.* [2002]. Thus, the altitude of the E2 wave peak in the GPH field (first row, right) coincides approximately with the altitude of the minimum between the double-peak structure in the temperature (fourth row, right). The altitude structure of the E2 wave in the NH (left column) is not so well outlined, but in general, it amplifies at higher altitudes than those in the SH. While the E2 wave in the GPH has the largest amplitude of 0.11 km at an altitude of ~ 70 km, those in the meridional and zonal winds have 6.6 m/s at $\sim 65\text{--}70$ km and 5.9 m/s at ~ 65 km, respectively. The E2 wave in the temperature has also a double-peak structure, but it is not very clear because the wave is weak, with the largest amplitude of 2.5 K. Additionally, the NH E2 wave has comparable amplitudes in the two consecutive winter periods, January–March 2009 and October 2009 to February 2010 and the occurring of the major SSW events in both winters disrupts its presence.

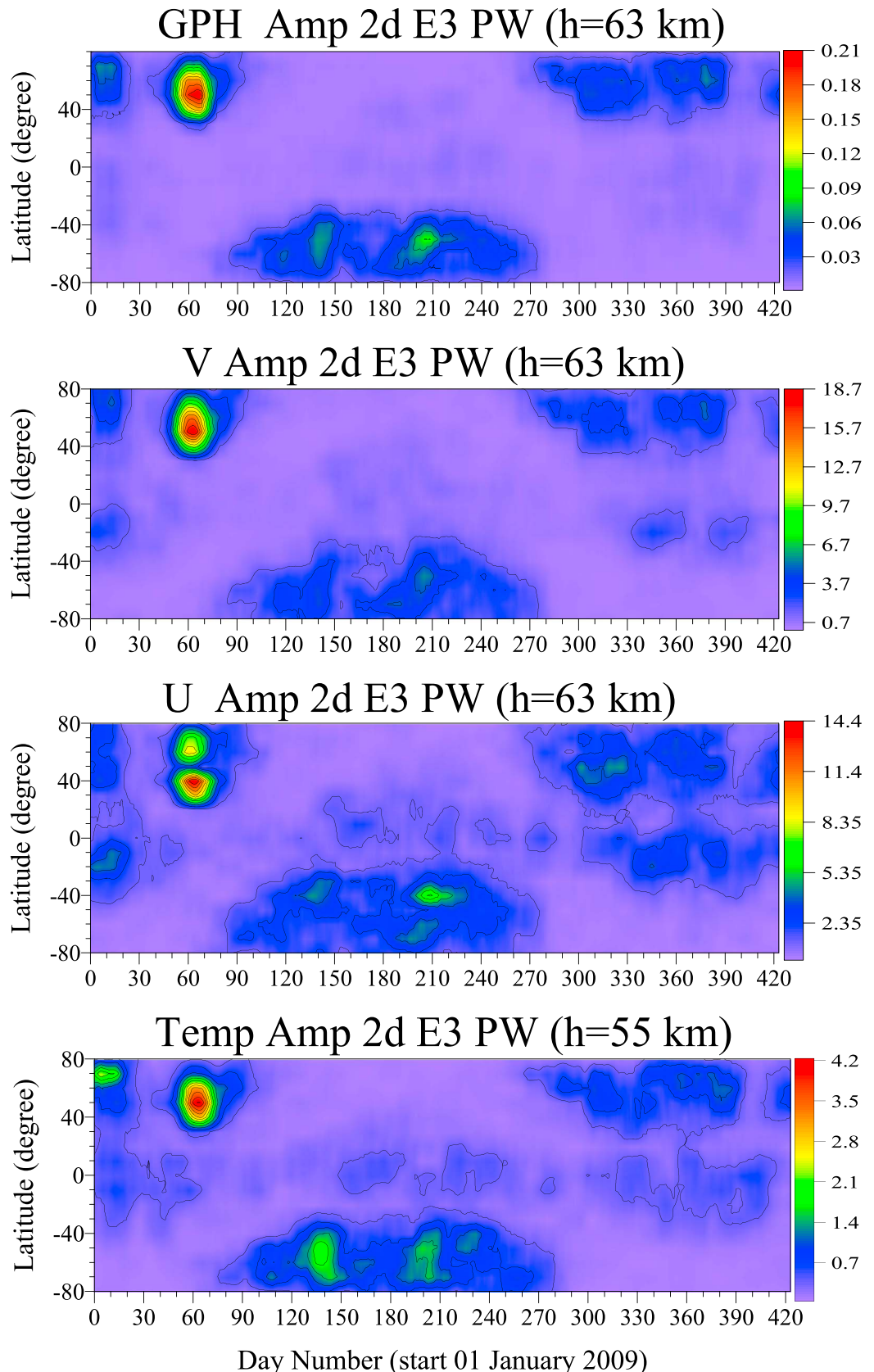


Figure 4. The same as Figure 3 but for the 2 day E3 wave amplitudes.

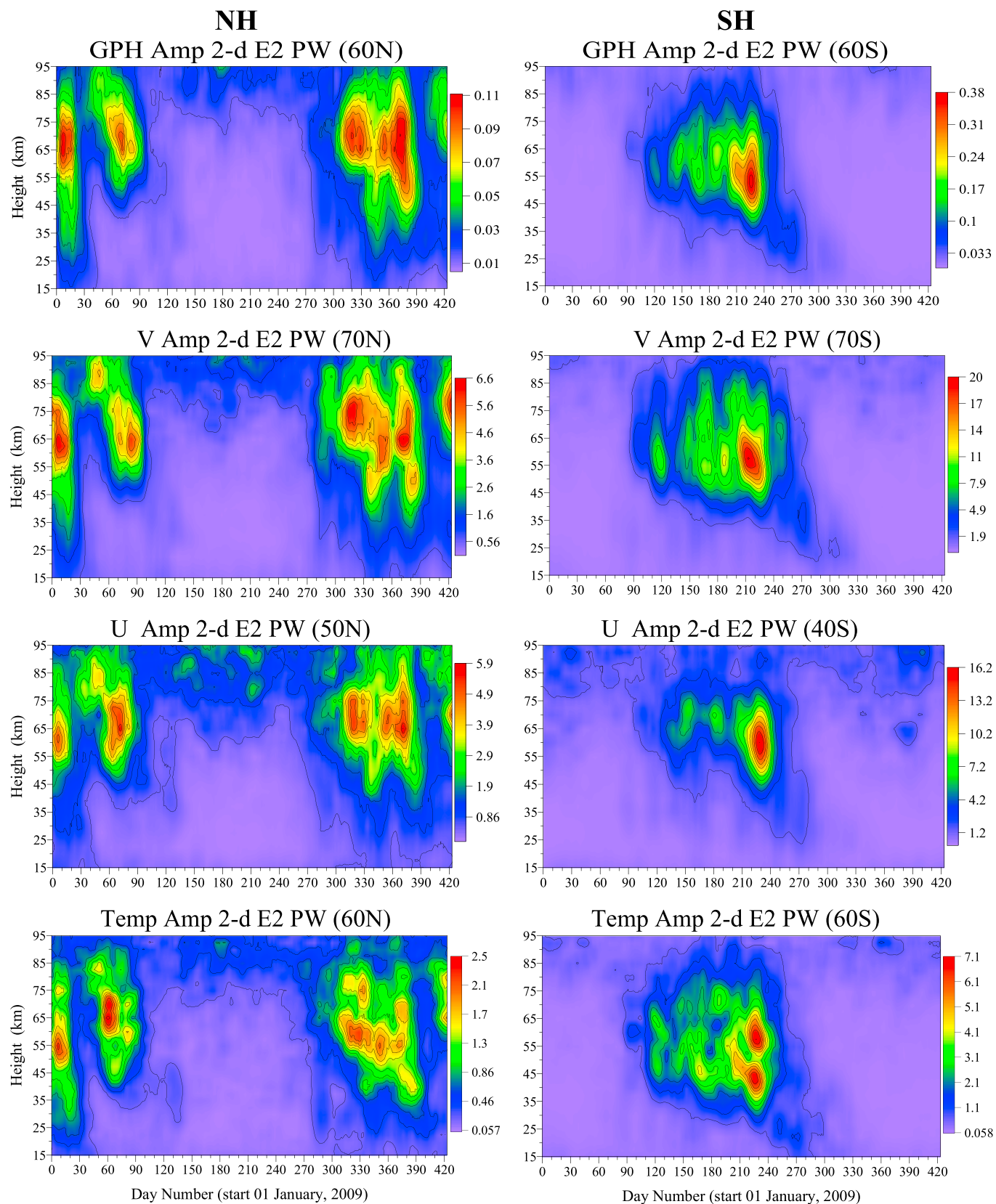


Figure 5. Altitude-time cross sections of the 2 day E2 wave amplitudes observed in the (first row) GPH, (second row) meridional wind, (third row) zonal wind, and (bottom row) temperature for the latitudes of the (left column) NH and (right column) SH which are marked at the upper side of each plot.

Figure 6 displays the same as Figure 5 but for the 2 day E3 wave amplitudes. In this case the E3 wave is significantly stronger (by at least 2 times) in the NH in all meteorological fields. The E3 wave maxima in the NH are situated around 60–65 km height, while in the SH they are at ~65–70 km for all meteorological fields except the temperature where a double-peak structure with maxima at ~55 and 70 km is seen again. The following largest amplitudes are seen in the NH: 0.20 km in the GPH, 17.3 m/s in the meridional wind, 12.4 m/s in the zonal wind, and 4.4 K in the temperature. The E3 wave is very strong in February/March 2009, but it is quite weak in the next boreal winter, October 2009 to February 2010; then its amplitude is on the average 3 times smaller. Two clear E3 wave bursts are seen in the SH centered near days 120–150 (May) and 180–210 (July); the second burst is stronger in all fields except in the temperature. The following largest amplitudes seen in the SH are as follows: 0.09 km in the GPH, 8.1 m/s in the meridional wind, 7.8 m/s in the zonal wind, and 2.3 K in the temperature.

It is worth noting that the comparison between the E2 and E3 waves in this data set reveals that the E2 wave in the SH is stronger than the E3 one in the NH in all meteorological fields although the maximum meridional wind speeds in the two hemispheres are almost the same.

3.3. Altitude and Latitude Structures of the E2 Wave Observed Over the Equator

The 2-D wavelet analysis has presented evidence for the presence of the E2 wave over the equator (see Figure 2). Figure 7 (left column) presents the latitude-time cross sections of the 2 day E2 wave amplitudes observed in the GPH at altitude of 95 km (top), zonal wind at altitude of 91 km (middle), and temperature at altitude of 85 km (bottom). The amplitudes (Figure 7) and phases (shown below) of all of the meteorological fields indicate that E2 wave is an equatorially trapped wave. The evidence from Figure 7 is that the amplitudes are almost symmetric about the equator and confined to the range $\pm(20\text{--}30^\circ)$. All plots show also the presence of weaker E2 wave perturbations at high latitudes observed in the local winter (already presented in sections 3.1 and 3.2); later, it will be demonstrated that the 2 day E2 wave over the equator and that at high latitudes are different types of wave.

Figure 7 (right column) shows the altitude-time cross sections of the 2 day E2 wave amplitudes observed in the GPH (top), zonal wind (middle), and temperature (bottom) over the equator (actually at 01°N). Again, similar variations are seen in all fields. The strongest E2 waves are observed in June–August in all fields; this could be partly related to the variability of the wave period, which is close to 2 days during these months (Figure 2b) and therefore is best captured by the spectral analysis using a fixed 48 h period. The E2 wave maximizes at different altitudes for the different fields; while it has the largest amplitude of 0.12 km at or above 95 km height in the GPH, in the zonal wind, and temperature the amplitudes are 10 m/s at ~90 km and 3.5 K at ~85 km, respectively. Besides the main amplification, the E2 wave has also a secondary one that can be seen at ~77–78 km in the GPH, ~80 km in the zonal wind, and ~75 km in the temperature.

It is worth mentioning that the analysis also shows a weak 2 day E3 wave at low latitudes, but it is at least 2–3 times weaker than the E2 wave and will not be investigated here.

3.4. Altitude- Latitude Structures of the E2 and E3 Waves

The waves are characterized not only by their amplitudes but by their phases as well. The phase behavior of the eastward traveling QTDWs is studied here by considering the altitude-latitude wave structure. In this way the relationship particularly between the equatorially trapped and high-latitude E2 waves will be seen as well. It has been already shown that due to both approximate geostrophic equilibrium and hydrostatic equation, the zonal wind and temperature perturbations, respectively, are related to the geopotential ones. This means that the single-peak latitudinal structure of the wave in the GPH defines the double-peak one in the zonal wind, and the single peak altitude structure of the wave in the GPH defines the double-peak one in the temperature. Due to this, only the E2 and E3 waves in the GPH data are presented here.

Figure 8a displays the altitude-latitude cross sections of the 2 day E2 wave amplitude (top row) and phase (in degrees, bottom row) observed in the GPH. The altitude-latitude structure is calculated for a period of time when the E2 wave at high latitude is strong; for the NH it is days 1–20 (January 2009), and for the SH it is 215–240 (August) as marked at upper side of each panel. The high-latitude E2 wave in the NH is situated at $\sim70^\circ\text{N}$ and maximizes at altitude of ~65 km, while that in the SH is located at $\sim60^\circ\text{S}$ and altitude of ~50 km. The E2 wave over the equator can be distinguished as well; for these periods it is weaker than that at high latitudes. The vertical phase variability reveals that both E2 waves (over the equator and at high

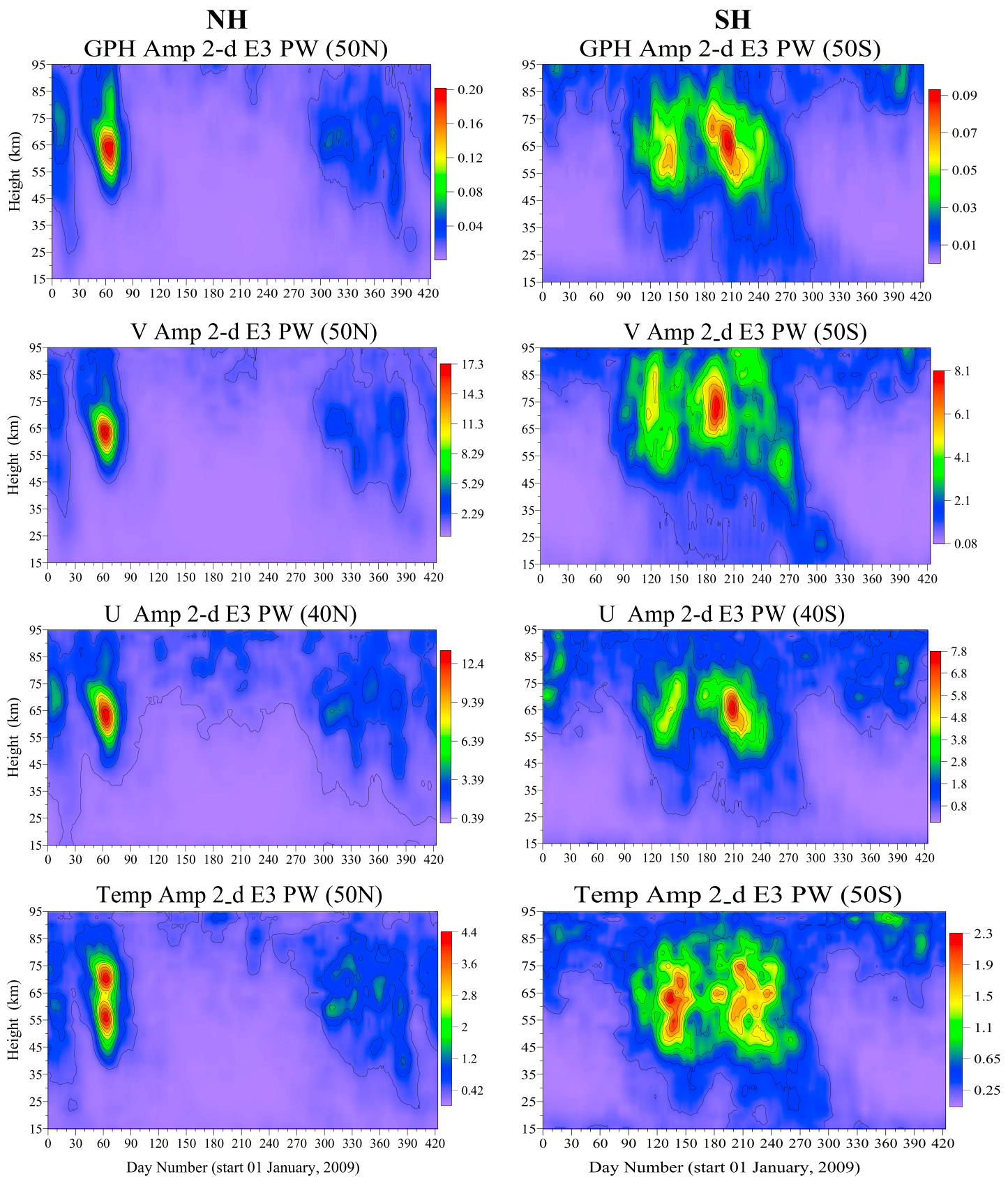


Figure 6. The same as Figure 5 but for the 2 day E3 wave amplitudes.

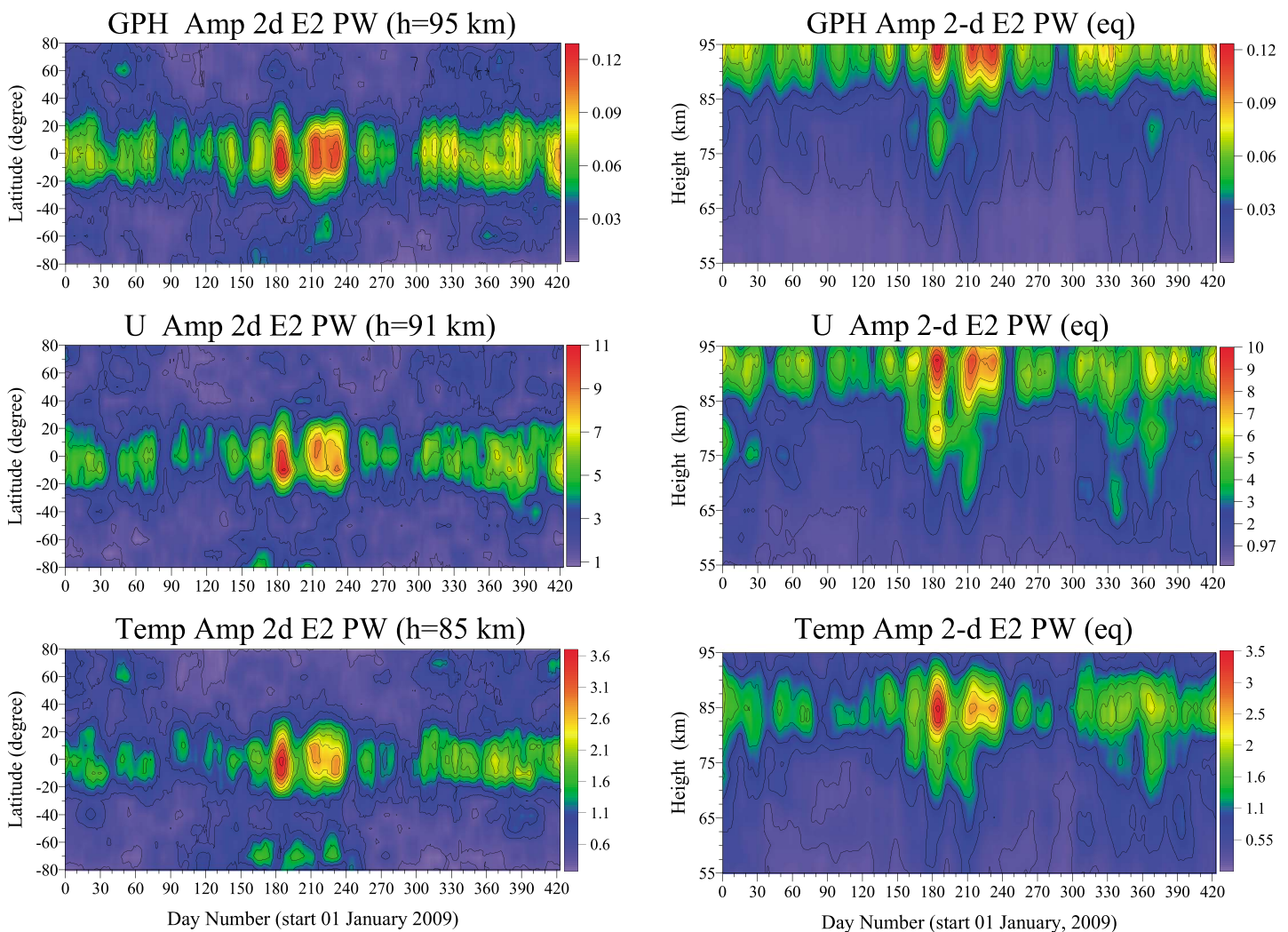


Figure 7. (left column) Latitude-time cross sections of the 2 day E2 wave amplitudes observed in the GPH at altitude of (top) 95 km, zonal wind at altitude of (middle) 91 km, and temperature at altitude of (bottom) 85 km. (right column) Altitude-time cross sections of the 2 day E2 wave amplitudes observed in the GPH (top), zonal wind (middle), and temperature (bottom) over the equator (01°N).

latitudes) are vertically upward propagating waves at least up to 85–90 km height. However, two distinct E2 phase structures are clearly seen in Figures 8a and 8b (bottom rows). The phases of the equatorially trapped E2 wave are uniform with latitude in the range of $\pm 30^{\circ}$. The vertical upward phase progression is well evident from the bottom of the altitude range analyzed (15 km), and the vertical wavelength is $\sim 30\text{--}35$ km. During both time intervals, January 2009 and August, this wave propagates up to ~ 90 km; above this level it becomes evanescent (the phase lines become vertical). The vertical propagation of the high-latitude E2 wave is seen from an altitude of ~ 25 km in the NH and ~ 20 km in the SH and continues up to $\sim 80\text{--}85$ km height; after that it becomes evanescent. The vertical wavelength of the high-latitude E2 wave is significantly larger than that over the equator; it is $\sim 60\text{--}65$ km.

Figure 8b shows the same as Figure 8a but for the E3 wave. The time intervals when the E3 wave is strong are as follows: days 50–70 (February/March) for the NH and 180–210 (July) for the SH. The NH high-latitude E3 wave has the largest amplitude at latitude of $\sim 50^{\circ}\text{N}$ and at altitude of ~ 65 km, while that in the SH is located at $\sim 50^{\circ}\text{S}$ and maximizes at ~ 70 km height. Their vertical upward propagation is seen from altitude of ~ 35 km up to ~ 85 km in both hemispheres, i.e., the E3 vertical wavelength is ~ 50 km. The plots show also weak E3 wave observed at low latitudes; in February/March this wave is almost centered over the equator; however, in July it is moved to 10°S . Their vertical phase structure reveals upward propagation from the lower

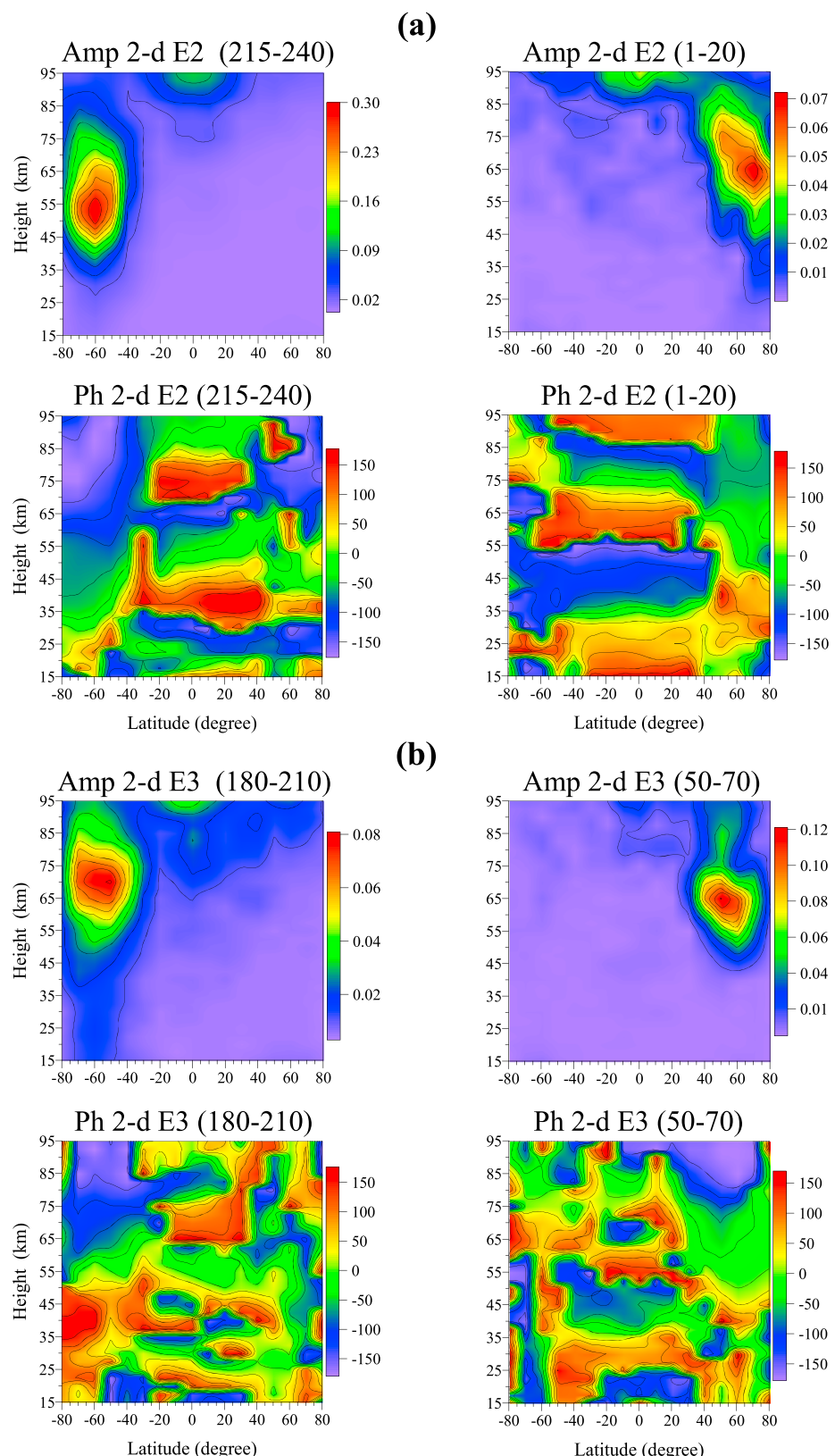


Figure 8. (a) Altitude-latitude cross sections of the 2 day E2 wave amplitude (top row) and phase (bottom row) observed in the GPH. (b) The same as Figure 8a but for the 2 day E3 wave. The time intervals for averaging are shown at the upper side of each plot.

stratospheric levels, but it is different from that of the E3 wave at high latitudes. The vertical wavelength is shorter than that at high latitudes and changes between ~ 15 and ~ 20 km. The E3 phase structure at low latitudes, particularly in July, does not resemble that of the equatorially trapped wave; the phase changes with latitude.

4. Westward Traveling QTDWs

In most of the papers devoted to the QTDW, westward traveling waves are described as dominant phenomena in the MLT during summer. Many studies describe the westward traveling QTDWs W2, W3, and W4 observed mainly in middle/high latitudes. The basic features of these waves are to some extent known; for completeness their presence in the NOGAPS-ALPHA meteorological fields will be shown here briefly. Only the waves in the GPH and meridional wind are presented.

Figure 9 presents the latitude-time cross sections of the 2 day W2 (left column), W3 (middle column), and W4 (right column) wave amplitudes observed in the geopotential height (top row) and meridional wind (bottom row). The latitudinal structures of these waves are shown at altitudes (marked at the upper side of each plot) where their amplitudes reach approximately the largest magnitudes. The following main features can be distinguished in both meteorological fields: (i) with increasing wave number, the waves amplify closer to the equator, i.e., while the W2 wave maximizes at $\pm (50\text{--}60^\circ)$ the W3 and W4 waves have the largest amplitudes near $\pm (40\text{--}50^\circ)$ and $\pm (30\text{--}40^\circ)$ respectively; (ii) there is a clear difference between the 2 day W2 waves in meridional wind at middle and equatorial latitudes; (iii) the W3 wave over the equator in the meridional wind, found by the wavelet analysis (see Figure 2a, bottom) and reported first by Wu *et al.* [1993], is seen here as an equatorward continuation of the midlatitude W3 wave.

Figure 10a shows the altitude-time cross sections of the 2 day W2 wave amplitudes observed in the GPH (top row) and meridional wind (bottom row) for the latitudes of the NH (left column) and SH (right column) which are marked at the upper side of each plot. Figures 10b and 10c display the same as Figure 10a but for the 2 day W3 and W4 waves, respectively. The main features seen in the altitude structures are the following. (i) With increasing wave number, the waves amplify at lower altitudes, i.e., while the W2 waves have the largest amplitude at or above 95 km height the W3 and W4 waves enhance around levels of $\sim 90\text{--}95$ km and $\sim 80\text{--}85$ km, respectively. The exception to this is that the W4 wave in the meridional wind amplifies around 90 km in January 2009. (ii) The W3 is the strongest westward traveling wave in both hemispheres and both meteorological fields. The largest amplitudes are 0.52 km in the GPH and 44 m/s in the meridional wind. In the NH for both fields the W4 wave is stronger than the W2; for SH, however, the W4 is stronger than the W2 only for the meridional wind, while for the GPH the opposite relation is seen. (iii) In the NH the main amplification of the W2 wave for both fields is near days 170–200, while those of the W3 and W4 waves can be seen around days 180–210 and 210–240, respectively. In the SH all waves enhance mainly in January 2009 during the first austral summer, while in the second summer the W2 and W4 are maximum in January 2010, but the W3 is maximum in February 2010. (iv) In the NH weak westward traveling waves are seen also in winter. The wintertime W3 and W4 waves are on the average an order of magnitude weaker than those during the summer (i.e., they are negligible), but the winter W2 wave is only 3–4 times weaker than the summertime one. A careful inspection indicates that the wintertime enhancement of the westward waves coincides with the two major SSW events in January 2009 and January 2010 and the minor one around mid-December 2009. Some weak amplification of the wintertime W2 wave is seen also in the SH stratosphere, around 30–35 km height, during the days 240–270; this stratospheric wintertime W2 enhancement will be considered below.

The wavelet analysis revealed the presence of the westward traveling waves W1, W2, and W3 in the meridional wind over the equator (see Figure 2a). While the W3 wave at tropical latitudes was reported first by Wu *et al.* [1993] and later considered in other studies, the 2 day W1 and W2 waves over the equator have not previously been reported in global meridional wind data. Figure 11a displays the latitude structure of the 2 day W1 wave amplitudes found in the meridional wind at altitude of ~ 90 km (top) and the altitude structure (bottom) over the equator (at 01°N). It is seen that this is an equatorially trapped wave, $\pm (20\text{--}30^\circ)$, which has the largest amplitude around 90 km height. Since its average period is ~ 45 h, the amplitudes obtained by the decomposition procedure with a fixed period of 48 h are slightly underestimated. Figure 11b shows the altitude-latitude cross sections of the 2 day W1 wave amplitude (top) and phase (in degrees, bottom) in the meridional wind and averaged for the days 370–390 when the W1 wave is quite strong. The altitude

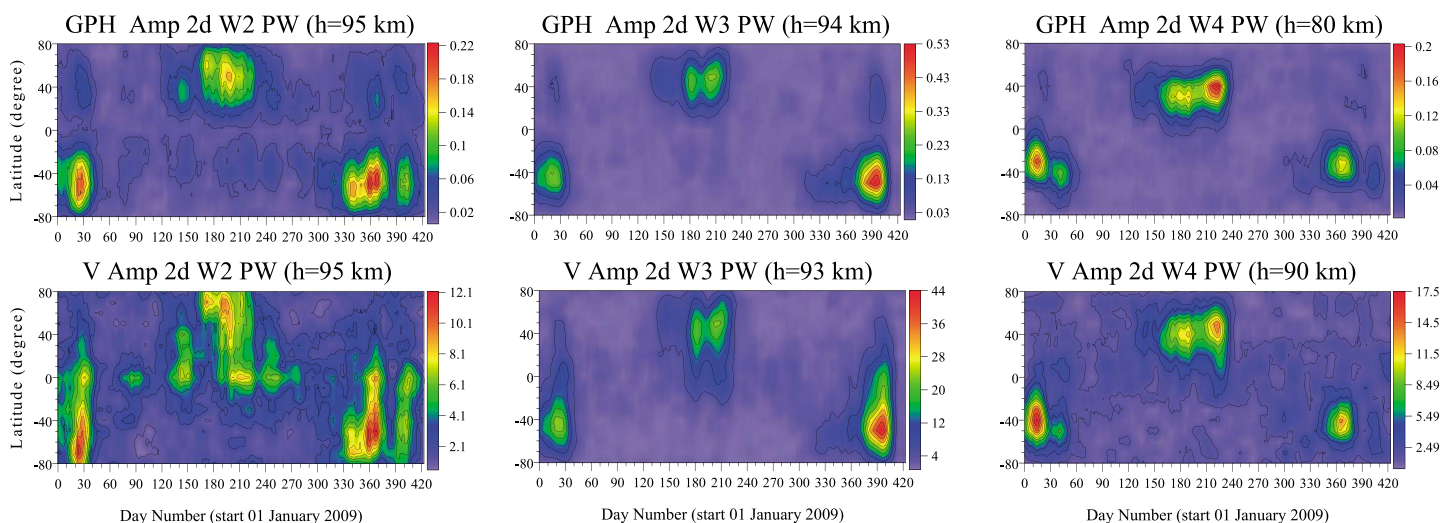


Figure 9. Latitude-time cross sections of the 2 day (left column) W2, (middle column) W3, and (right column) W4 wave amplitudes observed in the (top row) geopotential height and (bottom row) meridional wind at altitudes marked at the upper side of each plot.

phase structure indicates that this wave is vertically upward propagating wave practically over the entire altitude range shown and has a mean vertical wavelength of ~ 25 km. There is no latitudinal variation of the W1 wave phase, which is a clear indication that this wave is equatorially trapped.

Figure 12a shows the latitude (top) structure the 2 day W2 wave amplitude observed in the meridional wind at altitude of ~ 88 km and altitude (bottom) one over the equator. This wave at tropical latitudes has the largest amplitudes (~ 13.6 m/s) between 85 and 90 km and, in general, it is stronger than the midlatitude W2 wave particularly in the NH where the largest amplitude is ~ 9.5 m/s. The W2 wave at tropical latitudes amplifies considerably during both the two boreal winters (2009 and 2009–2010) and the summer (July/August), i.e., during the periods when the midlatitude W2 wave amplifies as well. However, there are other periods of amplifications which are not related to respective enhancements of the midlatitude W2 wave (for example, near days 80–100, 130–150, and 230–250). Figure 12b shows the altitude-latitude cross sections of the 2 day W2 wave amplitude (top row) and phase (bottom row) in the meridional wind and averaged for the days 360–380 (left column) and days 180–210 (right column) when the W2 wave is strong not only over the equator but also in the SH and NH, respectively. While there is a region of lower amplitude that allows the middle-/high-latitude W2 wave at around 70° N to be distinguished from the tropical wave in the amplitude plot (top row, right), there is no similar break in the SH between the tropics and the wave at 70° S (top row, left). The phase structures in both hemispheres show vertical upward propagation better seen in the SH (bottom row, left) above ~ 60 km height. Since the vertical phase gradient varies with altitude and the phases do not span an entire cycle (360°), we cannot determine a vertical wavelength. The high-latitude W2 wave in the NH (right column) shows some downward phase progression, but the wavelength cannot be assessed as well.

Figure 13a presents the altitude-latitude cross sections of the 2 day W3 wave amplitude (top row) and phase (bottom row) observed in the meridional wind; the time intervals for averaging are shown at the upper side of each plot. The amplitude plots of the W3 wave at both hemispheres reveal again that particularly in the upper mesosphere the tropical W3 wave is an equatorward continuation of the midlatitude W3 wave; below ~ 60 – 65 km; however, this wave is seen mainly at the tropics. The vertical phase structure shows some upward propagation particularly above ~ 60 km height, but the vertical wavelength cannot be assessed. Figure 13b shows the same as Figure 13a but for the 2 day W4 wave. Similarly to the W3 wave, the W4 phase structure indicates upward propagation above ~ 60 km height, but again, the vertical wavelength cannot be calculated from its vertical phase gradient.

Gu et al. [2016] investigated the QTDWs observed in January and February 2007 austral summer in a reanalysis produced by the data assimilation version of the Whole Atmosphere Community Climate Model (WACCM + Data Assimilation Research Testbed). The authors found that the W2, W3, and W4 waves

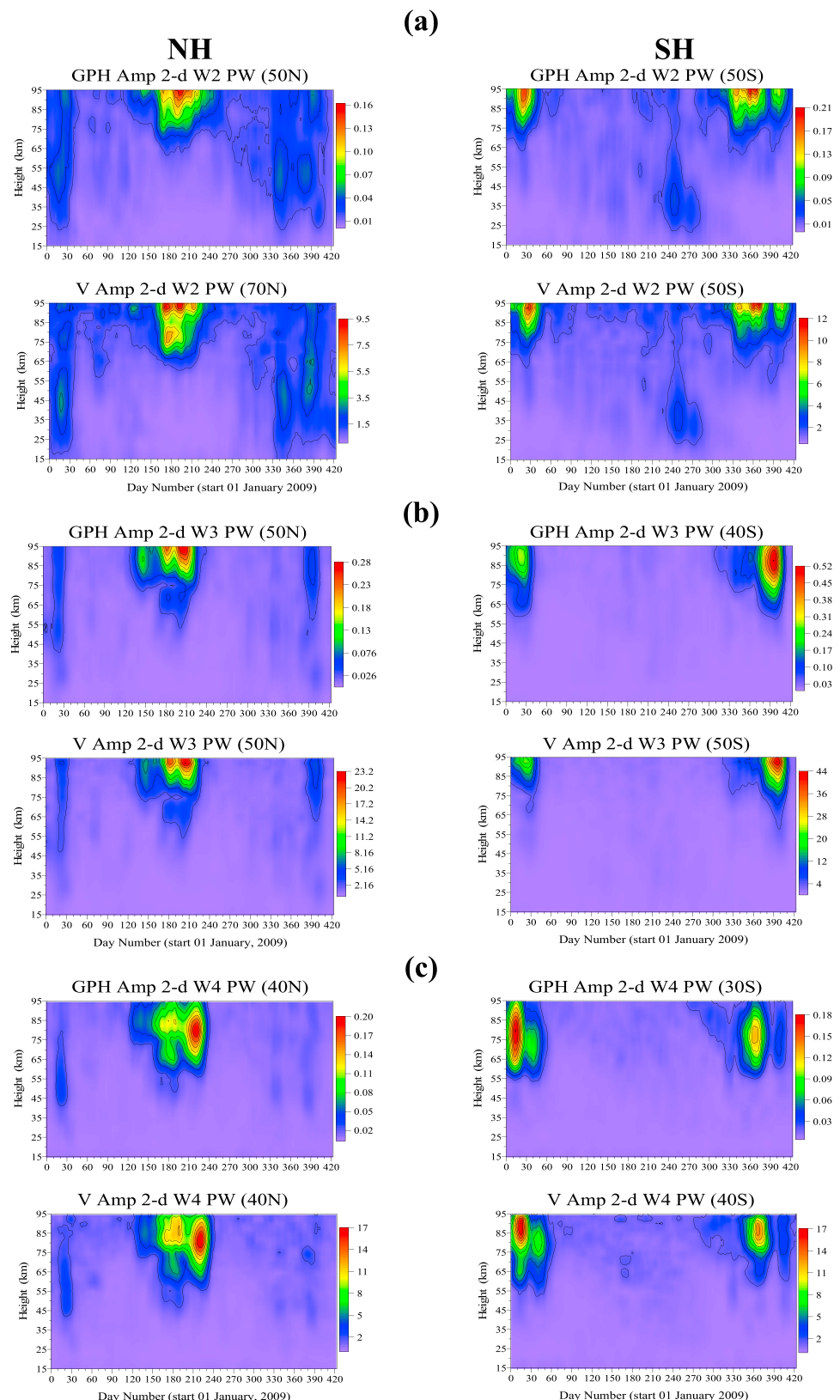


Figure 10. (a) Altitude-time cross sections of the 2 day W2 wave amplitudes observed in the GPH (top row) and meridional wind (bottom row) for the latitudes of the NH (left column) and SH (right column) which are marked at the upper side of each plot. (b) The same as Figure 10a but for the 2 day W3 wave. (c) The same as Figure 10a but for the 2 day W4 wave.

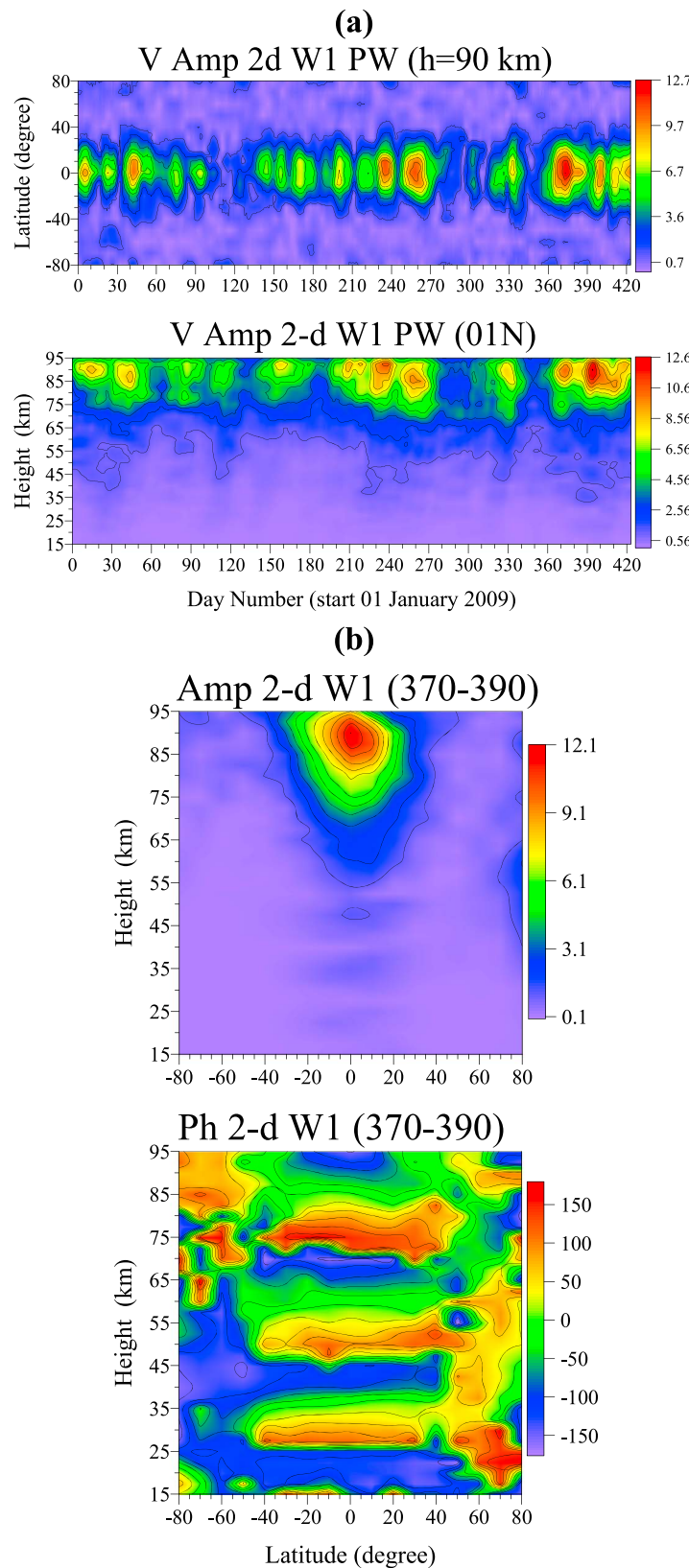


Figure 11. (a) Latitude (top) and altitude (bottom) structures of the 2 day W1 wave amplitudes observed in the meridional wind. (b) Altitude-latitude cross sections of the 2 day W1 wave amplitude (top) and phase (bottom) observed in the meridional wind and averaged for the days 370–390.

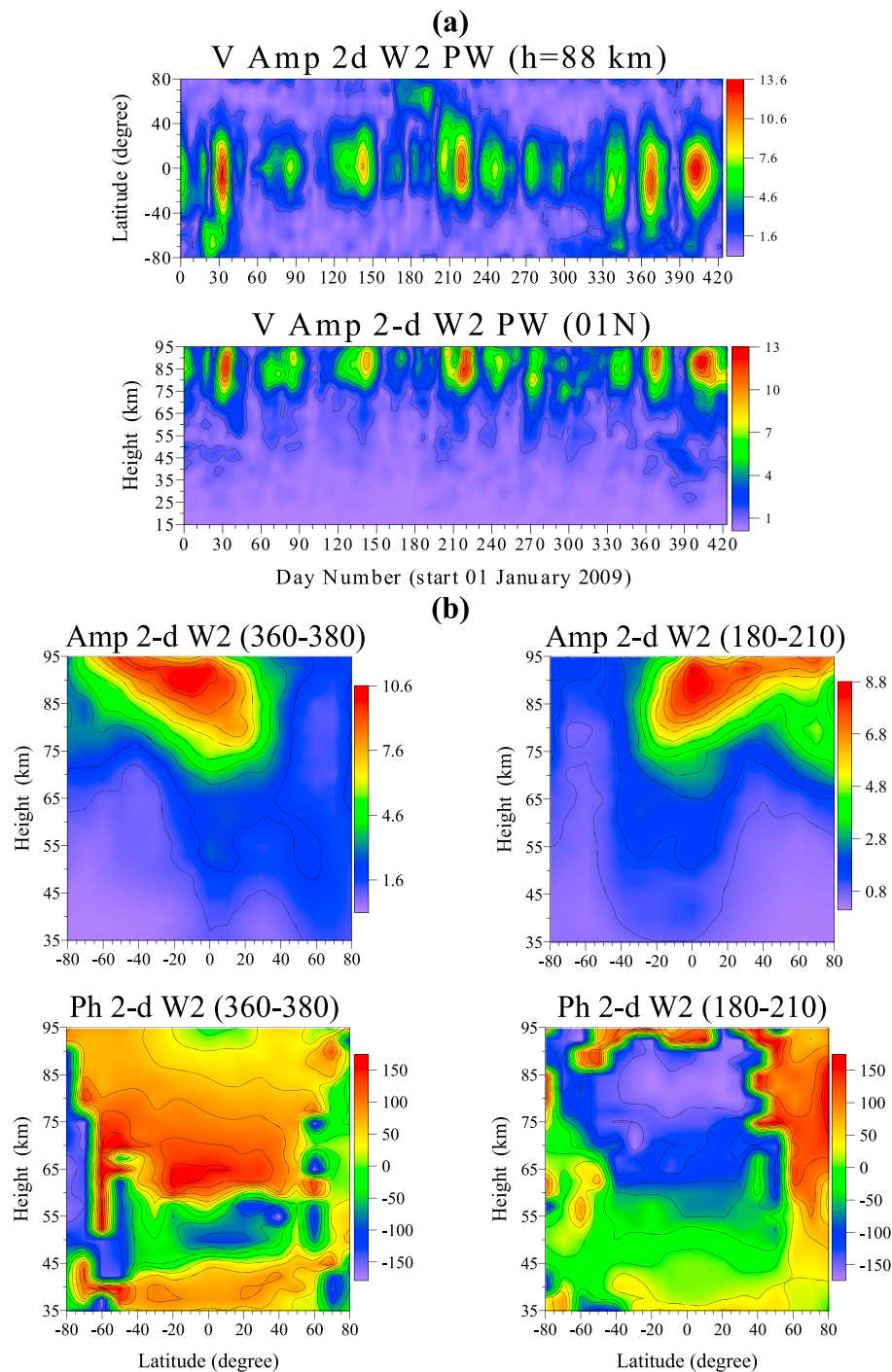


Figure 12. (a) Latitude (top) and altitude (bottom; above the equator) structures of the 2 day W2 wave amplitude observed in the meridional wind. (b) Altitude-latitude cross sections of the 2 day W2 wave amplitude (top row) and phase (bottom row) observed in the meridional wind; the time intervals for averaging are shown at the upper side of each plot.

propagate from NH (winter) to SH (summer) in the lower atmosphere, around 30–40 km height, where then they are amplified by the mean flow instabilities related to the summer easterly jet. We decided also to check if, in this reanalysis model data, the sources for the summertime westward traveling waves can be found in the opposite (winter) hemisphere. Figure 14a presents the temporal variations of the GPH perturbations of the 2 day W2 (top), W3 (middle), and W4 (bottom) at altitude of ~30 km. Two main features can be

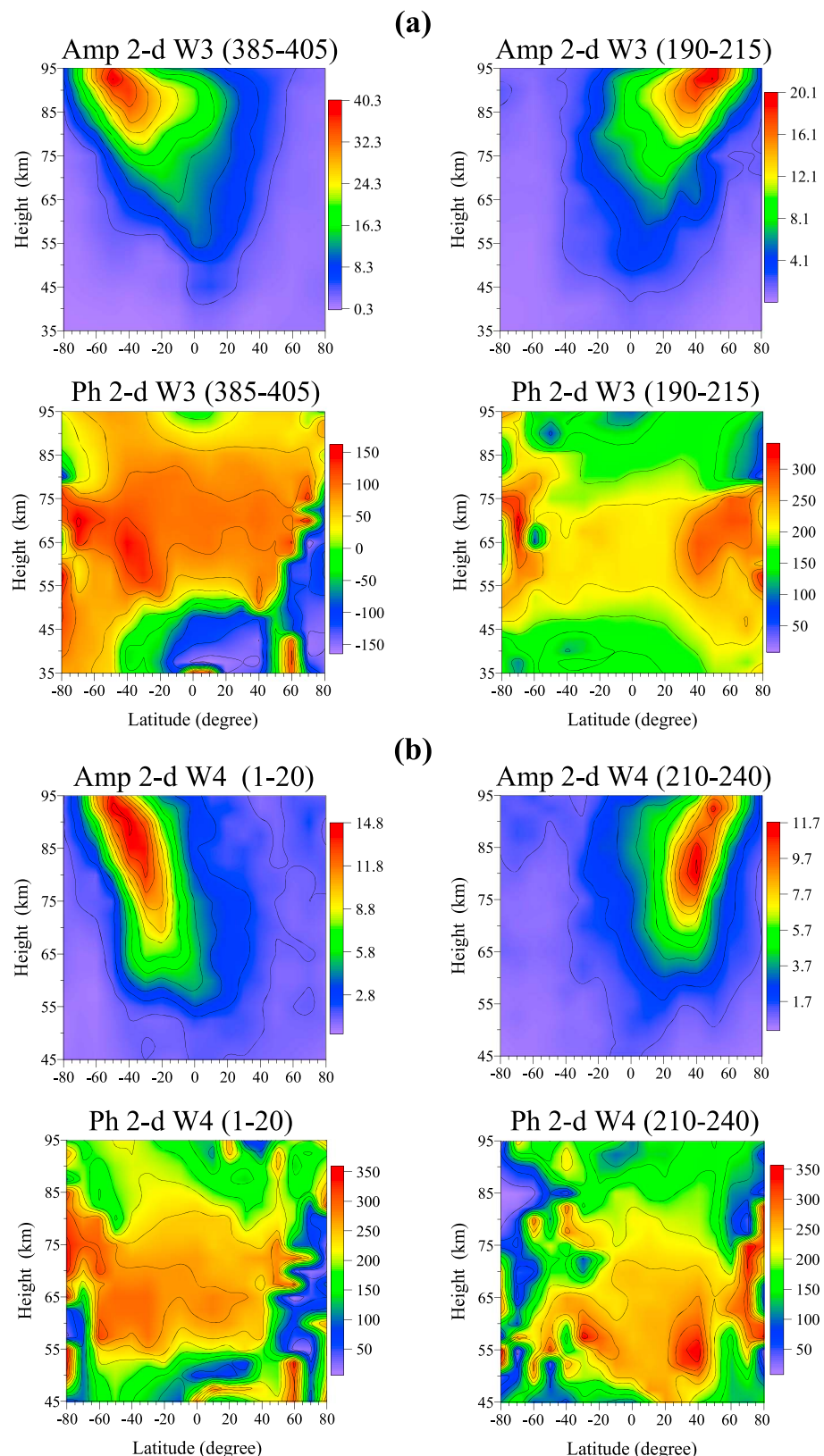


Figure 13. (a) Altitude-latitude cross sections of the 2 day W3 wave amplitude (top row) and phase (bottom row) observed in the meridional wind. (b) The same but for the 2 day W4 wave. The time intervals for averaging are shown at the upper side of each plot.

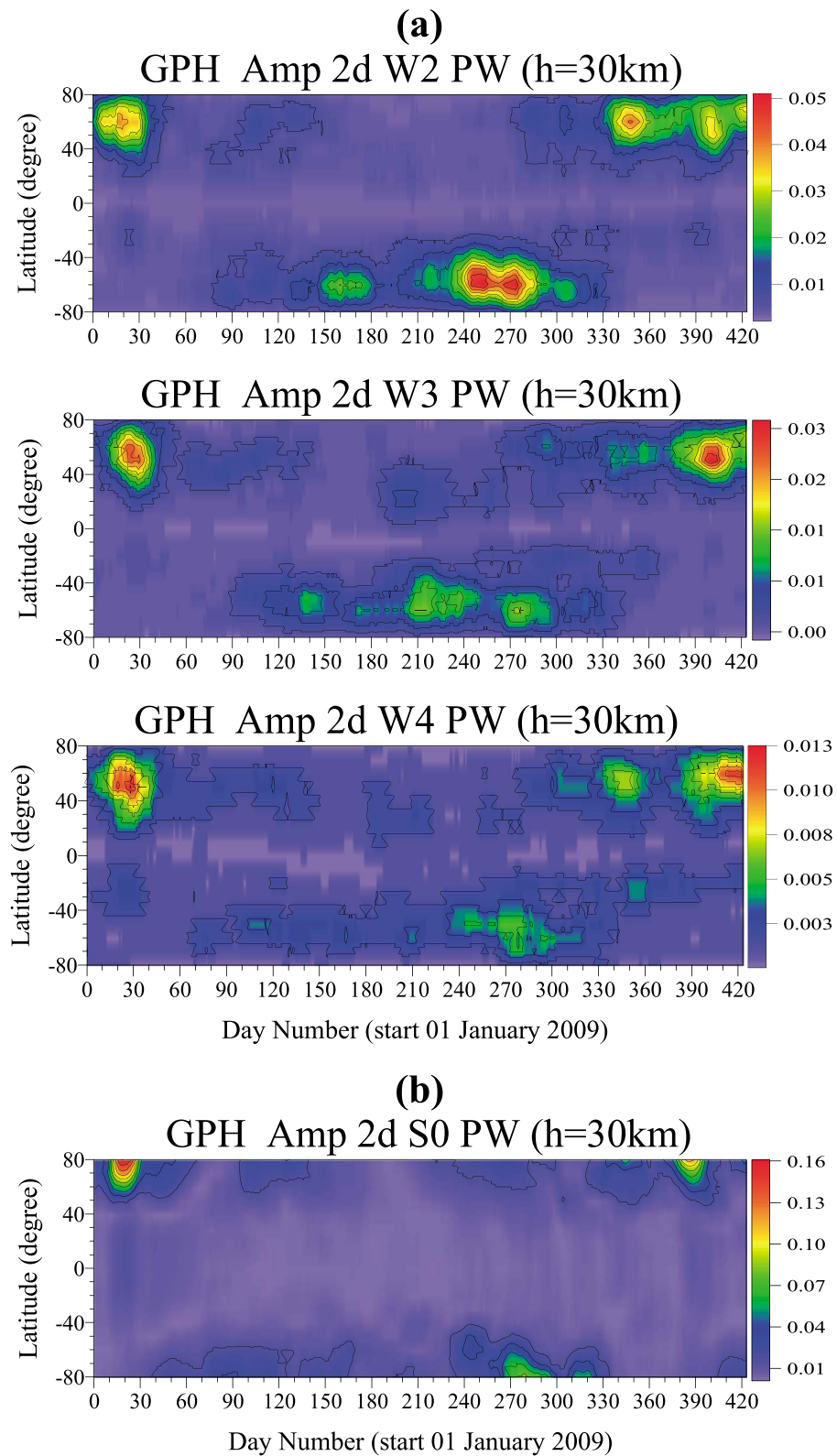


Figure 14. (a) The temporal variations of the GPH perturbations of the 2 day W2 (top), W3 (middle), and W4 (bottom) at altitude of 30 km. (b) The same as Figure 14a but for the 2 day S0 wave.

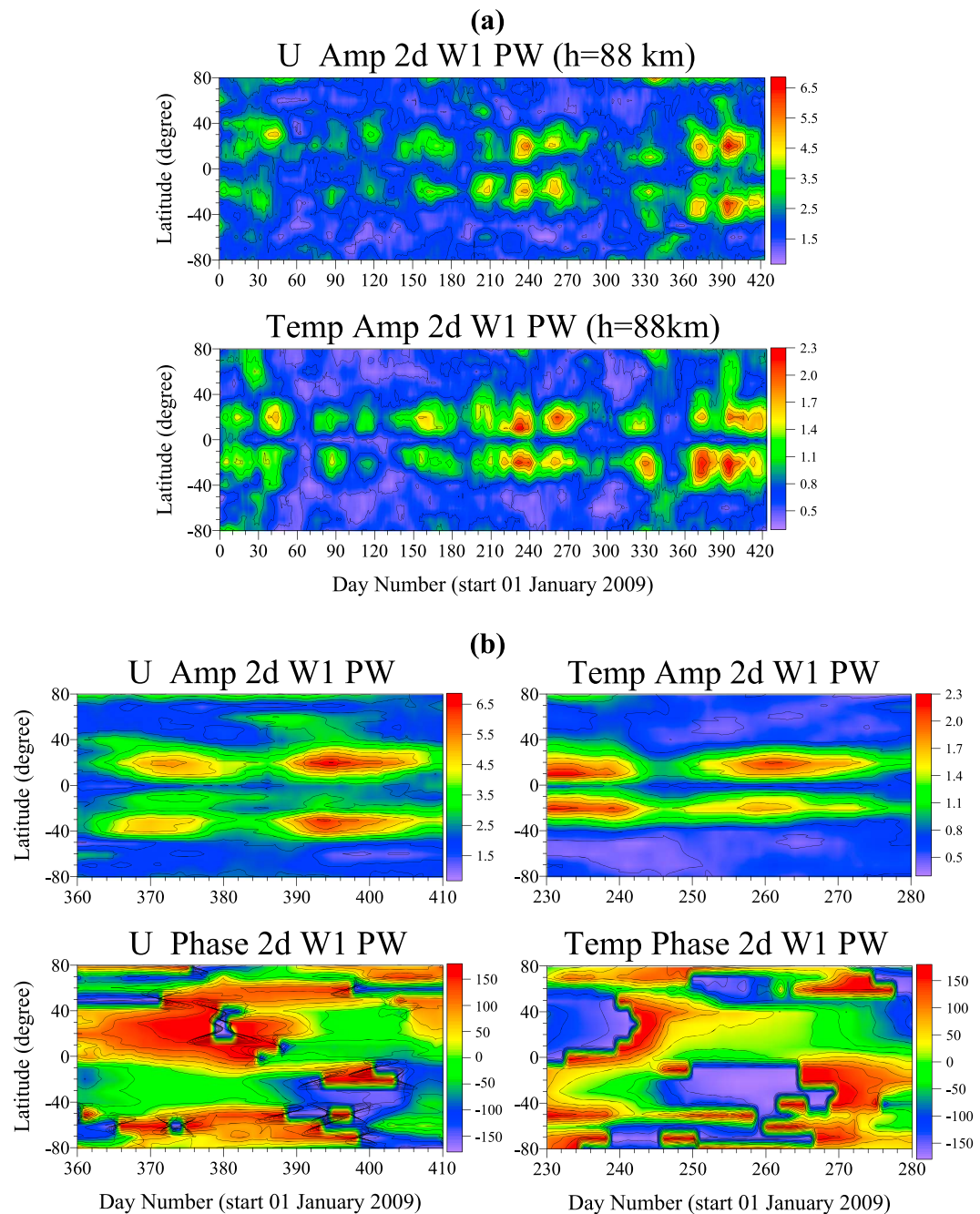


Figure 15. (a) Latitude-time cross sections of the 2 day W1 wave amplitudes observed in the zonal wind (top) and temperature (bottom) at altitude of ~ 88 km. (b) Latitude-time cross sections of the 2 day W1 amplitude (top row) and phase (bottom row) observed in the zonal wind (left column) during days 360–410 and in the temperature (right column) during days 230–280.

distinguished from these plots: (i) the source of the NH summertime (June–August) westward waves is situated in the SH (winter) high-latitude (~ 60 – 70° S) stratosphere, while that of the SH summertime (January–February) waves is located in the NH (winter) high-latitude (~ 50 – 70° N) stratosphere around 10 hPa, and (ii) the amplifications of the NH stratospheric W2, W3, and W4 perturbations (sources) coincides with the two major SSWs in January/February 2009 and 2010 and with the minor SSW in mid-December 2009.

During the above SSW events, an additional ~ 2 day wave is enhanced only at very high latitudes, $\pm 80^\circ$, which defines the short-term day-to-day variability of the zonal mean meteorological fields; this is a zonally

symmetric ($s=0$) 2 day wave. This wave is well evident in all fields except meridional wind. Figure 14b shows the temporal variations of the GPH perturbation of the 2 day S0 wave at altitude of ~ 30 km; its amplifications coincide with those of the amplifications of the wintertime westward waves (Figure 14a), i.e., with the above mentioned SSW events. The 2 day S0 wave in the GPH has its largest amplitude of 0.26 km (quite strong wave) around 50 km height.

In this section all westward traveling QTDWs have been considered. While the main features of the middle-/high-latitude waves observed during the local summer have been known from previous studies, those of the tropical W1 and W2 waves are presented here for the first time. It is worth mentioning also that the tropical W3 wave, particularly in the upper mesosphere, has been found here as an equatorward continuation of the midlatitude W3 wave, not as a secondary peak as in the satellite observations reported by Wu *et al.* [1993], Ward *et al.* [1996], or the simulations by the TIME-general circulation model reported by Yue *et al.* [2012]. Most probably, this is due to the altitude limitation (only up to ~ 95 km) of the NOGAPS-ALPHA data.

5. Discussion and Summary

This study presents the analysis of 14 months (January 2009 to February 2010) of continuous hourly NOGAPS-ALPHA reanalysis data used for examining the QTDWs. These data include information from satellite data that have been assimilated but have the significant advantages with respect to the direct satellite measurements that they give continuous global coverage, high temporal resolution, and suffer less from aliasing. These features make them suitable for investigating burst-like waves as the QTDWs. It is worth noting that even though the NOGAPS-ALPHA reanalysis model provides output in a regular grid, the fact that it is assimilating satellite data that suffer from aliasing might affect in some way the model output as well. In order to minimize the possible aliasing, the decomposition procedure applied in this study, where all tides and planetary waves are simultaneously separated from the data, is performed in UT.

The global structure and seasonal variability of the QTDWs in all meteorological fields (GPH, zonal and meridional wind, and temperature) have been studied. The wave characteristics are presented in latitude range $\pm 80^\circ$ and altitudes from 15 to 95 km. It is worth noting that the QTDWs are extracted from the data concurrently with the atmospheric tides and other planetary waves. In this way both tides and QTDWs are not mutually affected.

Two different types of eastward traveling waves are identified: (i) waves at middle and high latitudes which are observed in the local winters and (ii) waves observed predominantly over the equator, which do not have a well-defined seasonal variability but show some enhancement between June and August. While the first type of waves is seen in all meteorological fields, the second ones are not seen in the meridional wind.

The wintertime QTDW event in both hemispheres is composed of E2 and E3 waves. While the E2 wave is significantly stronger in the SH than that in the NH, for the E3 wave an opposite relation is seen: it is stronger in the NH than that in the SH. This is found for E2 and E3 waves in all meteorological fields. These are vertically upward propagating waves with vertical wavelength $\sim 60\text{--}65$ km for the E2 wave and ~ 50 km for the E3 one. These waves are generated in the stratosphere, $\sim 20\text{--}30$ km for the E2 wave and $\sim 35\text{--}40$ km for the E3 one, and propagate vertically up to ~ 90 km; after that they become evanescent. We found also that the major SSW events in January 2009 and 2010 disrupt the existence of the eastward traveling waves because the winter eastward zonal mean flow is replaced by the westward one and then the zonal mean wind circulation will not satisfy the Charney and Drazin [1961] criterion. Sandford *et al.* [2008] identified a 2 day E2 wave in the geopotential height MLS/Aura measurements with the largest amplitude of 0.15 km for the NH and typical vertical wavelength of ~ 125 km. The result for the E2 amplitude is close to that presented here, 0.11 km (Figure 5, top row left); however, the vertical wavelength they found is 2 times larger than that from our analysis, $\sim 60\text{--}65$ km.

An important problem is to clarify the mechanisms for generating the E2 and E3 waves. Two mechanisms have been proposed for the excitation of the 2 day E2 wave in the middle atmosphere. By numerical simulations performed with a simple nonlinear model Merzlyakova and Pancheva [2007] found that the appearance of the eastward traveling ~ 2 day wave with zonal wave number 2 at mesospheric heights can be forced mainly by the jet instability in the stratosphere. The present result for the 2 day E2 wave shows that this wave originates in the lower to middle stratosphere ($\sim 20\text{--}30$ km height), maximizes at $\sim 55\text{--}65$ km and propagates

vertically upward to ~90 km, providing coupling of these layers. The other eastward traveling E3 wave is probably generated also by instabilities in the polar night jet; however, modeling studies are necessary to clarify its generation mechanism. In some cases the 2 day E3 wave could be generated also by a nonlinear interaction between the 2 day E2 wave with the SPW1.

Another driving mechanism of the 2 day E2 wave is attributed to a nonlinear coupling between the 2 day W3 wave and the migrating (W1) diurnal tide [Palo *et al.*, 2007]. The 2 day E2 wave generated by this mechanism is observed during the local summer when the 2 day W3 is significantly enhanced. It is worth noting, however, that the 2 day E2 wave determined from analysis of satellite data could be strongly affected by aliasing.

The second type of eastward traveling waves found in the present study is that of waves seen at low latitudes; these are E2 and E3 waves. Only the E2 wave has been examined in detail here because it is well defined and is at least 2.5–3 times stronger than the E3 one. The E2 wave is seen in all meteorological fields except the meridional wind. It is equatorially trapped wave, almost symmetric about the equator and located in the latitude range \pm (20–30°). It is a vertically upward propagating wave with vertical wavelength of ~30–35 km. According to its features, the E2 wave can be interpreted as a Kelvin wave. Additional evidence is the approximate satisfaction of the dispersion relation [Holton *et al.*, 2001]:

$$\lambda_z = T_N \left[\frac{\lambda_x}{T_{E2}} - \bar{u} \right]$$

where T_N is the Brunt-Väisälä period (it is ~300 s in the MLT region), T_{E2} is the period of 2 day E2 wave (~48 h), and λ_x is the horizontal wavelength (~20,000 km for the wave number 2). This wave is particularly strong in July–August when the zonal mean zonal wind is about -(5–10) m/s. Actually, the contribution of the zonal mean zonal wind is generally small. The approximate satisfaction of the dispersion relation is strong evidence that the 2 day E2 wave is an ultrafast Kelvin wave.

Two different types of westward traveling waves have been identified as well: (i) waves at middle and high latitudes which are observed mainly in summer hemisphere and (ii) waves observed predominantly over the equator, enhanced predominantly at both solstices but are seen in other seasons as well. While the first type waves are seen in all meteorological fields, the second ones are observed in the meridional wind.

It has been already mentioned that the westward traveling waves observed in middle/high latitudes during summer (W2, W3, and W4 modes) have been quite extensively investigated. Most of the reported features are seen in the NOGAPS-ALPHA model data as well. An important feature clearly demonstrated here is that at increasing wave number the westward modes amplify closer to the equator and at lower heights.

The W3 is the strongest mode in both hemispheres and all meteorological fields; it is followed by the W4 mode, and the weakest one is W2; the exception is that in the SH the W2 in the GPH is stronger than the respective W4 mode. Gu *et al.* [2016] found that the QTDW peaked 3 times from January to February 2007 but with different zonal wave numbers, while the W2 mode maximized in the first half of January, the W3 and W4 modes peaked in late January and late February, respectively. However, our results for the SH (see Figure 10, right column) revealed that all three modes enhance in January 2009, while W2 and W4 amplify in January 2010 and W3 in February 2010. If we consider the strongest peak of each westward traveling mode in the NH (see Figure 10, left column), then it can be distinguished that the W2 peak maximizes around day 180, while the W3 and W4 ones have the largest amplitudes near days 200 and 225. The latitude-altitude structures of the above modes (see Figures 12b and 13) show that, in general, they are vertically upward propagating waves, particularly above 60–65 km height. We, however, were not able to estimate their precise vertical wavelengths.

The second type of westward traveling waves found in the present study is that of waves seen at low latitudes in meridional wind; these are W1, W2, and W3 waves. The low-latitude W3 wave has been already reported and identified as a Rossby-gravity (3, 0) mode, while the W1 and W2 waves have not been found, so far, in global meridional wind data. Their existence however was predicted by Pancheva *et al.* [2006] through analyzing the perturbations in the geomagnetic field measured in 23 stations situated at low latitudes. The authors found 2 day variations in the ionospheric electric currents identified as westward propagating global 2 day waves with zonal wave numbers 1 and 2.

It has been found that the 2 day W1 wave is an equatorially trapped wave, \pm (20–30°), which has the largest amplitude around 90 km height. This is vertically upward propagating wave practically through all the

altitude range with a mean vertical wavelength of ~ 25 km. Our analysis shows that it is consistent with an identification as a Rossby-gravity (1, 0) mode due to the following characteristics: (i) the meridional wind has a maximum amplitude over the equator, while temperature and zonal wind have maximum amplitudes on either side of the equator, and (ii) the wave is asymmetric with respect to the equator, i.e., the perturbations on opposite sides of the equator are out of phase. This is demonstrated in Figures 15a and 15b. Figure 15a shows latitude-time cross sections of the 2 day W1 wave amplitudes observed in the zonal wind (top) and temperature (bottom) at altitude of ~ 88 km; it is seen that the W1 wave amplifies at both sides of the equator, but just over the equator it is absent. Figure 15b presents again latitude-time cross subsections of the 2 day W1 amplitude (top row) and phase (bottom row) observed in the zonal wind (left column) during days 360–410, and in the temperature (right column) during days 230–280; the time intervals shown correspond to periods when the W1 wave has the largest amplitude. The phase plots present evidence that the W1 is asymmetric with respect to the equator.

The W2 wave is also a Rossby-gravity mode, and this can be noticed in Figure 9 (left column). The W2 meridional wind has maximum over the equator, and its GPH amplifies on both sides of the equator. The latitude structures of the W2 wave in temperature and zonal wind are very similar to those of the W1 wave shown in Figure 15 and due are not shown here. In studying the vertical phase structures of both the middle-/high- and the low-latitude W2 waves we have not been able to establish a complete distinction between the two waves, particularly in the SH, nor to estimate their precise vertical wavelengths. This will be further investigated in the near future as a case study of two austral summer periods of January and February 2005 and 2008; observations indicate that the W2 waves in both latitude regions are significantly stronger than those in the 2009–2010 period investigated in the present study.

It is worth noting that the found in this study new Rossby-gravity W1 and W2 waves are particularly important for the coupling of the atmosphere-ionosphere system because these 2 day waves are equatorially trapped and directly can have impact on the vertical plasma drift.

Summarizing, we note that this study provides reliable new insight into the eastward and westward traveling QTDWs in the middle atmosphere between ~ 15 km and 95 km height. The use of hourly reanalysis data, which suffer less from aliasing than do the original satellite data, allows a comprehensive understanding of the global spatial-temporal QTDW distribution by simultaneous separations of all tides and planetary waves. These results could be used as a solid base for searching for such waves in other atmospheric global data, particularly from middle atmosphere research satellites.

Acknowledgments

D.E.S. acknowledges support from the NASA Living with a Star program (inter-agency agreement NNN13AW411 to the Naval Research Laboratory). The hourly NOGAPS-ALPHA product is publicly available via anonymous FTP from map.nrl.navy.mil/pub/nrl/nogaps. The National Center for Atmospheric Research (NCAR) is sponsored by the U.S. National Science Foundation (NSF). This work was supported by the European Office of Aerospace Research and Development (EOARD), Air Force Office of Scientific Research, Air Force Material Command, USAF, under grant number FA8655-12-1-2057 to D.P. We thank the anonymous reviewers for their insightful comments on the original manuscript.

References

- Altadill, D., and E. Apostolov (1998), Vertical development of the 2-day wave in the midlatitude ionospheric F-region, *J. Geophys. Res.*, **103**, 29,199–29,206, doi:10.1029/1998JA900004.
- Apostolov, E. M., D. Altadill, and L. F. Alberca (1995), Characteristics of quasi-2-day oscillations in the f_0F_2 at northern middle latitude, *J. Geophys. Res.*, **100**, 12,163–12,171, doi:10.1029/95JA00134.
- Burks, D., and C. B. Leovy (1986), Planetary waves near the mesospheric easterly jet, *Geophys. Res. Lett.*, **13**, 193–196, doi:10.1029/GL013i003p00193.
- Charney, J. G., and P. G. Drazin (1961), Propagation of planetary-scale disturbances from the lower into the upper atmosphere, *J. Geophys. Res.*, **66**, 83–109, doi:10.1029/JZ066i001p00083.
- Chen, P.-R. (1992), Two day oscillation of the equatorial ionization anomaly, *J. Geophys. Res.*, **97**, 6343–6357, doi:10.1029/91JA02445.
- Coy, L. (1979), A possible 2-day wave oscillation near the tropical stratopause, *J. Atmos. Sci.*, **36**, 1615–1618, doi:10.1175/1520-0469(1979)036<1615:APDONT>2.0.CO;2.
- Coy, L., S. D. Eckermann, and K. Hoppel (2009), Planetary wave breaking and tropospheric forcing as seen in the stratospheric sudden warming of 2006, *J. Atmos. Sci.*, **66**, 495–507, doi:10.1175/2008JAS2784.1.
- Craig, R. L., R. A. Vincent, G. J. Fraser, and M. H. Smith (1980), The quasi-2-day wave in the Southern Hemisphere mesosphere, *Nature*, **287**, 319–320, doi:10.1038/287319a0.
- Eckermann, S. D., K. W. Hoppel, L. Coy, J. P. McCormack, D. E. Siskind, K. Nielsen, A. Kochenash, M. H. Stevens, and C. R. Englert (2009), High-altitude data assimilation system experiments for the Northern Hemisphere summer mesosphere season of 2007, *J. Atmos. Sol. Terr. Phys.*, **71**, 531–551, doi:10.1016/j.jastp.2008.09.036.
- Forbes, J. M., R. Guffe, X. Zang, D. Fritts, D. Riggan, A. Manson, C. Meek, and R. Vincent (1997), Quasi-2-day oscillation of the ionosphere during summer 1992, *J. Geophys. Res.*, **102**, 7301–7305, doi:10.1029/96JA01744.
- Garcia, R. R., R. Lieberman, J. M. Russell, and M. G. Mylne (2005), Large-scale waves in the mesosphere and lower thermosphere observed by SABER, *J. Atmos. Sci.*, **62**, 4384–4399, doi:10.1175/JAS3612.1.
- Gu, S.-Y., T. Li, X. Dou, Q. Wu, M. G. Mylne, and J. M. Russell (2013), Observations of quasi-two-day wave by TIMED/SABER and TIMED/TIDI, *J. Geophys. Res. Atmos.*, **118**, 1624–1639, doi:10.1002/jgrd.50191.
- Gu, S.-Y., H.-L. Liu, T. Li, X. Dou, Q. Wu, and J. M. Russell (2015), Evidence of nonlinear interaction between quasi 2 day wave and quasi stationary wave, *J. Geophys. Res. Space Physics*, **120**, 1256–1263, doi:10.1002/2014JA020919.
- Gu, S.-Y., H.-L. Liu, N. M. Pedatella, X. Dou, T. Li, and T. Chen (2016), The quasi 2 day wave activities during 2007 austral summer period as revealed by Whole Atmosphere Community Climate Model, *J. Geophys. Res. Space Physics*, **121**, 2743–2754, doi:10.1002/2015JA022225.

- Gurubaran, S., S. Sridharan, T. K. Ramkumar, and R. Rajaram (2001a), The mesospheric quasi-2-day wave over Tirunelveli (8.7°N), *J. Atmos. Sol. Terr. Phys.*, **63**, 975–985, doi:10.1016/S1364-6826(01)00016-5.
- Gurubaran, S., T. K. Ramkumar, S. Sridharan, and R. Rajaram (2001b), Signatures of quasi-2-day planetary waves in the equatorial electrojet: Results from simultaneous observations of mesospheric winds and geomagnetic field variations at low latitudes, *J. Atmos. Sol. Terr. Phys.*, **63**, 813–821, doi:10.1016/S1364-6826(00)00193-0.
- Harris, T. J., and R. A. Vincent (1993), The quasi-2-day wave observed in the equatorial middle atmosphere, *J. Geophys. Res.*, **98**, 10,481–10,490, doi:10.1029/93JD00380.
- Holton, J. R., M. J. Alexander, and M. T. Boehm (2001), Evidence for short vertical wavelength Kelvin waves in the Department of Energy-Atmospheric Radiation Measurement Nauru99 radiosonde data, *J. Geophys. Res.*, **106**, 20,125–20,130, doi:10.1029/2001JD900108.
- Ito, R., S. Kato, and T. Tsuda (1986), Consideration of an ionospheric wind dynamo driven by a planetary wave with a two-day period, *J. Atmos. Terr. Phys.*, **48**, 1–13, doi:10.1016/0021-9169(86)90108-X.
- Kal'chenko, B. V., and S. V. Bulgakov (1973), Study of periodic components of wind velocity in the lower thermosphere above the equator, *Geomagn. Aeron.*, **13**, 955–956.
- Lieberman, R. S. (1999), Eliassen-Palm fluxes of the 2-day wave, *J. Atmos. Sci.*, **56**, 2846–2861, doi:10.1175/1520-0469(1999)056<2846:EPFOTD>2.0.CO;2.
- Lieberman, R. S., D. M. Riggan, D. A. Ortland, J. Oberheide, and D. E. Siskind (2015), Global observations and modeling of nonmigrating diurnal tides generated by tide-planetary wave interactions, *J. Geophys. Res. Atmos.*, **120**, 11,419–11,437, doi:10.1002/2015JD023739.
- Lima, L. M., P. P. Batista, H. Takahashi, and B. R. Clemesha (2004), Quasi-two-day observed by meteor radar at 22.7°S , *J. Atmos. Sol. Terr. Phys.*, **66**, 529–537, doi:10.1016/j.jastp.2004.01.007.
- Limasuvan, V., D. L. Wu, M. J. Schwartz, J. W. Waters, Q. Wu, and T. L. Killeen (2005), The two-day wave in EOS MLS temperature and wind measurements during 2004–2005 winter, *Geophys. Res. Lett.*, **32**, L17809, doi:10.1029/2005GL023396.
- Manson, A. H., C. E. Meek, C. M. Hall, S. Nozawa, N. J. Mitchell, D. Pancheva, W. Singer, and P. Hoffmann (2004), Mesopause dynamics from the Scandinavian triangle of radars within the PSMOS-DATAR Project, *Ann. Geophys.*, **22**, 367–386, doi:10.5194/angeo-22-367-2004.
- McCormack, J. P., L. Coy, and K. W. Hoppel (2009), Evolution of the quasi 2-day wave during January 2006, *J. Geophys. Res.*, **114**, D20115, doi:10.1029/2009JD012239.
- McCormack, J. P., S. D. Eckermann, K. W. Hoppel, and R. A. Vincent (2010), Amplification of the quasi-two day wave through nonlinear interaction with the migrating diurnal tide, *Geophys. Res. Lett.*, **37**, L16810, doi:10.1029/2010GL043906.
- Meek, C. E., et al. (1996), Global study of Northern Hemisphere quasi-2-day wave events in recent summers near 90 km altitude, *J. Atmos. Terr. Phys.*, **58**, 1401–1411, doi:10.1016/0021-9169(95)00120-4.
- Merzlyakova, E. G., and D. V. Pancheva (2007), The 1.5–5-day eastward waves in the upper stratosphere–mesosphere as observed by the Esrange meteor radar and the SABER instrument, *J. Atmos. Sol. Terr. Phys.*, **69**, 2102–2117, doi:10.1016/j.jastp.2007.07.002.
- Merzlyakov, E. G., Y. I. Portnyagin, N. A. Makarov, J. Forbes, and S. Palo (2005), Eastward-propagating day-to-day wind oscillations in the Northern Polar mesosphere/lower thermosphere, *Izv. Atmos. Ocean. Phys.*, **41**, 72–84.
- Moudden, Y., and J. M. Forbes (2014), Quasi-two-day wave structure, interannual variability, and tidal interactions during the 2002–2011 decade, *J. Geophys. Res. Atmos.*, **119**, 2241–2260, doi:10.1002/2013JD020563.
- Mukhtarov, P., B. Andonov, C. Borries, D. Pancheva, and N. Jakowski (2010), Forcing of the ionosphere from above and below during the Arctic winter of 2005/2006, *J. Atmos. Sol. Terr. Phys.*, **72**, 193–205, doi:10.1016/j.jastp.2009.11.008.
- Muller, H. G. (1972), Long-period meteor wind oscillations, *Philos. Trans. Roy. Soc. London*, **271**, 585–598, doi:10.1089/rsta.1972.0026.
- Niciejewski, R., W. Skinner, M. Cooper, A. Marshall, R. R. Meier, M. H. Stevens, D. Ortland, and Q. Wu (2011), Verification of large-scale rapid transport in the lower thermosphere: Tracking the exhaust plume of STS-107 from launch to the Antarctic, *J. Geophys. Res.*, **116**, A05302, doi:10.1029/2010JA016277.
- Nielsen, K., D. E. Siskind, S. D. Eckermann, K. W. Hoppel, L. Coy, J. P. McCormack, S. Benze, C. E. Randall, and M. E. Hervig (2010), Seasonal variation of the quasi 5 day planetary wave: Causes and consequences for polar mesospheric cloud variability in 2007, *J. Geophys. Res.*, **115**, D18111, doi:10.1029/2009JD012676.
- Norton, W. A., and J. Thuburn (1996), The two-day wave in a middle atmosphere GCM, *Geophys. Res. Lett.*, **23**, 2113–2116, doi:10.1029/96GL01956.
- Nozawa, S., H. Iwahashi, A. Brekke, C. M. Hall, C. Meek, A. Manson, S. Oyama, Y. Murayama, and R. Fujii (2003), The quasi 2-day wave observed in the polar mesosphere: Comparison of the characteristics observed at Tromso and Poker Flat, *J. Geophys. Res.*, **108(D24)**, 4748, doi:10.1029/2002JD003221.
- Palo, S. E., and S. K. Avery (1995), Observations of the meridional quasi-two-day wave in the mesosphere and lower thermosphere at Christmas Island, in *The Upper Mesosphere and Lower Thermosphere: A Review of Experiment and Theory*, *Geophys. Monogr. Series*, No 87, pp. 101–110, AGU, Washington, D. C.
- Palo, S. E., J. M. Forbes, X. Zhang, J. M. Russell, and M. G. Mlynczak (2007), An eastward propagating two-day wave: Evidence for nonlinear planetary wave and tidal coupling in the mesosphere and lower thermosphere, *Geophys. Res. Lett.*, **34**, L07807, doi:10.1029/2006GL027728.
- Pancheva, D. (2006), Quasi-2-day wave and tidal variability observed over Ascension Island during January/February 2003, *J. Atmos. Sol. Terr. Phys.*, **68**, 390–407, doi:10.1016/j.jastp.2005.02.028.
- Pancheva, D., and I. Lysenko (1988), Quasi-2-day fluctuations observed in the summer F region electron maximum, *Bulg. Geophys. J.*, **14**, 41–51.
- Pancheva, D., L. F. Alberca, and B. de la Morena (1994), Simultaneous observation of the quasi-2-day wave in the lower and upper ionosphere over Europe, *J. Atmos. Terr. Phys.*, **56**, 43–50, doi:10.1016/0021-9169(94)90174-0.
- Pancheva, D., et al. (2004a), Variability of the quasi-2-day wave observed in the MLT region during the PSMOS campaign of June–August 1999, *J. Atmos. Sol. Terr. Phys.*, **66**, 539–565, doi:10.1016/j.jastp.2004.01.008.
- Pancheva, D., N. Mitchell, and P. Younger (2004b), Meteor radar observations of atmospheric waves in the equatorial mesosphere/lower thermosphere over Ascension Island, *Ann. Geophys.*, **22**, 387–404, doi:10.5194/angeo-22-387-2004.
- Pancheva, D. V., et al. (2006), Two-day wave coupling of the low-latitude atmosphere-ionosphere system, *J. Geophys. Res.*, **111**, A07313, doi:10.1029/2005JA011562.
- Pfister, L. (1985), Baroclinic instability of easterly jets with applications to the summer mesosphere, *J. Atmos. Sci.*, **42**, 313–330, doi:10.1175/1520-0469(1985)042<0313:BIOEJW>2.0.CO;2.
- Plumb, R. A. (1983), Baroclinic instability of the summer mesosphere: A mechanism for the quasi-two-day wave?, *J. Atmos. Sci.*, **40**, 262–270, doi:10.1175/1520-0469(1983)040<0262:BIOTSM>2.0.CO;2.
- Raghava Reddi, C., A. Geetha, and K. R. Lekshmi (1988), Quasi-2-day wave in the middle atmosphere over Trivandrum, *Ann. Geophys.*, **6**, 231–238.

- Riggin, D. M., R. S. Lieberman, R. A. Vincent, A. H. Manson, C. E. Meek, T. Nakamura, T. Tsuda, and Y. I. Portnyagin (2004), The 2-day wave during the boreal summer of 1994, *J. Geophys. Res.*, **109**, D08110, doi:10.1029/2003JD004493.
- Rodgers, C. D., and A. J. Prata (1981), Evidence for a travelling 2-day wave in the middle atmosphere, *J. Geophys. Res.*, **86**, 9661–9664, doi:10.1029/JC086iC10p09661.
- Rojas, M., and W. Norton (2007), Amplification of the 2-day wave from mutual interaction of global Rossby-gravity and local modes in the summer mesosphere, *J. Geophys. Res.*, **112**, D12114, doi:10.1029/2006JD008084.
- Salby, M. L. (1981a), Rossby normal modes in nonuniform background configurations I, Simple fields, *J. Atmos. Sci.*, **38**, 1803–1826, doi:10.1175/1520-0469(1981)038<1803:RNMINB>2.0.CO;2.
- Salby, M. L. (1981b), Rossby normal modes in non-uniform background configurations II. Equinox and solstice conditions, *J. Atmos. Sci.*, **38**, 1827–1840, doi:10.1175/1520-0469(1981)038<1827:RNMINB>2.0.CO;2.
- Salby, M. L., and P. F. Callaghan (2001), Seasonal amplification of the 2-day wave: Relationship between normal mode and instability, *J. Atmos. Sci.*, **58**, 1858–1869, doi:10.1175/1520-0469(2001)058<1858:SAOTDW>2.0.CO;2.
- Sandford, D. J., M. J. Schwartz, and N. J. Mitchell (2008), The wintertime two-day wave in the polar stratosphere, mesosphere and lower thermosphere, *Atmos. Chem. Phys.*, **8**(3), 749–755, doi:10.5194/acp-8-749-2008.
- Sassi, F., R. R. Garcia, B. A. Boville, and H. Liu (2002), On temperature inversions and the mesospheric surf zone, *J. Geophys. Res.*, **107**(D19), 4380, doi:10.1029/2001JD001525.
- Siskind, D. E., M. H. Stevens, M. Hervig, F. Sassi, K. Hoppel, C. R. Englert, and A. J. Kochenash (2011), Consequences of recent Southern Hemisphere winter variability on polar mesospheric clouds, *J. Atmos. Sol. Terr. Phys.*, **73**, 2013–2021, doi:10.1016/j.jastp.2011.06.014.
- Siskind, D. E., D. P. Drob, J. T. Emmert, M. H. Stevens, P. E. Sheese, E. J. Llewellyn, M. E. Hervig, R. Niciejewski, and A. J. Kochenash (2012), Linkages between the cold summer mesopause and thermospheric zonal mean circulation, *Geophys. Res. Lett.*, **39**, L01804, doi:10.1029/2011GL050196.
- Stevens, M. H., et al. (2010), Tidally induced variations of polar mesospheric cloud altitudes and ice water content using a data assimilation system, *J. Geophys. Res.*, **115**, D18209, doi:10.1029/2009JD013225.
- Thayaparan, T., W. K. Hocking, and J. MacDougall (1997), Amplitude, phase and period variations of the quasi-2-day wave in the mesosphere and lower thermosphere over London, Canada (43°N , 81°W), during 1993 and 1994, *J. Geophys. Res.*, **102**, 9461–9478, doi:10.1029/96JD03869.
- Tunbridge, V. M., D. J. Sandford, and N. J. Mitchell (2011), Zonal wave numbers of the summertime 2 day planetary wave observed in the mesosphere by EOS Aura Microwave Limb Sounder, *J. Geophys. Res.*, **116**, D11103, doi:10.1029/2010JD014567.
- Walterscheid, R., and R. Vincent (1996), Tidal generation of the phase-locked 2-day wave in the southern hemisphere summer by wave-wave interactions, *J. Geophys. Res.*, **101**, 26,567–26,576, doi:10.1029/96JD02248.
- Ward, W. E., D. Y. Yang, B. H. Solheim, and G. G. Shepherd (1996), Observations of the 2-day wave in WINDII data during January 1993, *Geophys. Res. Lett.*, **23**, 2923–2926, doi:10.1029/96GL02897.
- Wu, D. L., P. B. Hays, W. R. Skinner, A. R. Marshall, M. D. Burrage, R. S. Lieberman, and D. A. Ortland (1993), Observations of the quasi-2-day wave from the high resolution Doppler imager, *Geophys. Res. Lett.*, **20**, 2853–2856, doi:10.1029/93GL03008.
- Wu, D. L., P. B. Hays, and W. R. Skinner (1995), A least squares method for spectral analysis of space-time series, *J. Atmos. Sci.*, **52**(20), 3501–3511, doi:10.1175/1520-0469(1995)052<3501:ALSMFS>2.0.CO;2.
- Yue, J., H.-L. Liu, and L. C. Chang (2012), Numerical investigation of the quasi 2 day wave in the mesosphere and lower thermosphere, *J. Geophys. Res.*, **117**, D05111, doi:10.1029/2011JD016574.
- Yue, J., W. Wang, A. D. Richmond, H.-L. Liu, and L. C. Chang (2013), Wavenumber broadening of the quasi-two-day planetary wave in the ionosphere, *J. Geophys. Res. Space Physics*, **118**, 3515–3526, doi:10.1002/jgra.50307.